CHAPTER 8
PERFORMANCE-LIMITING MAGNETOHYDRODYNAMICS IN JET

R. J. BUTTERY* and T. C. HENDER
EURATOM/UKAEA Fusion Association, Culham Science Centre
Abingdon, Oxfordshire OX14 3DB, United Kingdom

Received June 22, 2007
Accepted for Publication November 29, 2007

JET has made a strong contribution to the understanding of stability issues for the tokamak. An overview of its main achievements is presented, with emphasis on the latest progress in resolving the key issues for ITER. In particular, we conclude that control or avoidance strategies for neoclassical tearing modes (NTMs) will be necessary for good performance in ITER. JET studies have provided insights into the transport effects, seeding, underlying physics, and threshold scaling of NTMs. A range of mechanisms are found that can trigger performance-impacting NTMs with various mode numbers. Experiments have highlighted the key role of the sawtooth in triggering the NTM and have developed sawtooth control. The underlying physics suggests increased likelihood of NTM triggering as ITER scales are approached. Extensions have also been made in understanding of error field locked modes and resistive wall modes (RWMs). The predictions for ITER of error field locked mode thresholds have been developed and refined taking account of JET data. Direct inference from experimental studies and benchmarking of magnetohydrodynamic codes have both contributed to improved understanding of RWM stability in ITER. From these developments, and from the parameter space it accesses, JET continues to provide an essential role, and unique operating points, to further test and resolve the stability issues of tokamak physics.

KEYWORDS: *tokamak, fusion, stability*

Note: Some figures in this paper are in color only in the electronic version.

Contents—Chapter 8

*E-mail: richard.buttery@ukaea.org.uk

I. INTRODUCTION

I.A. Historical Perspective

From its earliest days of operation, the JET tokamak[1] has made a leading contribution toward the understanding of plasma instabilities, the processes involved, and the limits they impose on tokamak performance. Studies have explored a wide range of parameter space, first establishing the basic stable regions of operation and then exploring the detailed behavior of both the most serious events, such as disruptions, and other plasma instabilities that influence performance.

The first work explored the limits on density and plasma current, and it was found that pushing these parameters too far led to terminations of the discharge.[2] This density limit was consistent with previous understanding, seen as arising from increasing levels of radiative power.[3] When this exceeded the input heating power, the plasma edge would cool and begin to contract. This in turn would lower the effective edge safety factor, destabilizing the plasma to magnetohydrodynamic (MHD)

instabilities that would violently rearrange the plasma configuration, leading to termination via interactions with the vessel wall. The JET results provided clear data showing this contraction in the electron temperature profile, making the first step towards understanding this class of disruption. Exploration of the parameter space[4] showed how the density limit scaled effectively with the plasma current and also identified the limit in edge safety factor q_a corresponding to when a key rational flux surface $q = 2$ approaches the plasma edge and destabilizes a strong current gradient–driven instability.

The disruption processes were studied in considerable detail, with significant consequences identified both in forces arising from eddy currents induced in the vessel and in the potential for localized damage to the vessel wall arising from "runaway" electron beams and localized heating. A sequence of events leading to the disruption were identified: First, a tearing mode destabilizes the plasma, breaking magnetic symmetry and modestly reducing confinement; this triggers an impurity influx[5] from the wall that cools the plasma, causing the current to decay. Conservation of flux then drives image currents in surrounding conducting structures. Also identified were halo currents, which flow from the plasma through the vessel structure, leading to large, asymmetric, and potentially damaging forces on the device.

Another key field of development at JET was in the understanding and control of the sawtooth oscillation. These core instabilities arise from a build up of excess current in the plasma core. When the safety factor in this region falls significantly below 1, a fast reconnection of the plasma core is considered to expel the core. However, the event on JET (Refs. 6 and 7) occurred two orders of magnitude faster than theoretical predictions at that time, and with similar results obtained on other devices, this led to a debate for many years. It was resolved[8] by allowing for electron inertia in the essentially collisionless plasmas of JET, although questions still remained in explaining the postcrash state and degree of reconnection expected.

The sawtooth was to gain renewed interest at JET with the introduction of ion cyclotron resonant heating (ICRH). Above certain levels of power, the ICRH was found to lead to infrequent so-called "monster" events.[9] The explanation of this was quite simple—the fast particles generated by ICRH would stabilize the instability for a time, until the mode drives were too strong to be contained. This stabilization process was generated as a result of the conservation of magnetic flux encircled by the precessional drift orbits of the energetic ions, enabling them to suppress the sawteeth.[10] This poses a concern for burning plasma devices, in which fast particle populations would also be expected to partially stabilize sawteeth, leading to larger, more destructive events. In fact, as we discuss later in this chapter, the principal concern now comes from such sawteeth triggering secondary modes that degrade the confinement across a broader region of the plasma. It is feared that fast particle–stabilized sawteeth will excite a number of such modes readily, at relatively low β and with large amplitude—an effect directly observed with ion cyclotron resonance frequency (ICRF)-excited α particles already on JET (Ref. 11). Nevertheless, in the 1990s ICRH current drive techniques were shown to influence the sawtooth[12] by changing the local magnetic shear at the resonant $q = 1$ surface, providing the basis of a control technique that has now been developed to mainstream high-performance plasmas at JET today.[13,14]

More recently, studies have also explored a range of stability issues for so-called "advanced scenario" plasmas. These regimes deploy early heating to prevent full current penetration to the core of the plasma, thereby resulting in high amounts of off-axis current and increased values of central safety factor. The purpose of this is to provide access to plasma scenarios more suited for steady-state, fully noninductive operation, as described in Chap. 4 in this issue. In some variants of these regimes, these techniques result in a region of reversed shear in the plasma core, with a hollow safety factor (q) profile. As was shown in Ref. 15 (and references therein), this introduces additional classes of instability such as "double tearing" involving two resonant surfaces with the same rational q value, resistive interchange in reversed shear regions, and snakes in regions of very low magnetic shear at rational q. Such instabilities were found to have a range of performance-degrading effects on advanced scenarios. The authors showed that the optimization of the safety factor profile evolution is a crucial element in developing a stable path to high-performing reversed shear scenarios, particularly with regard to the occurrence of rational safety factor surfaces, and their timing. This work also identified the performance-limiting role of the pressure-driven kink on JET, which we discuss in the next section.

I.B. Key Instabilities of Concern for ITER

For a wider exploration of the basics and the pioneering work performed in the early phases of JET, we refer the reader to the excellent papers discussed above, and the references therein. In this chapter we now consider some of the more recent work that is at the forefront of considerations for future devices such as ITER and other burning plasma experiments. We concentrate on large-scale instabilities in the plasma core that can limit the main plasma scenarios; edge instabilities and finer-scale instabilities driven by fast particles are discussed in Chapters 3 and 5, respectively, of this issue.

The current primary concerns for next-step devices, from a stability perspective, arise principally from two types of instability—the tearing mode and the pressure-driven kink instability. These occur in different parameter regions and so account for limits in different scenarios. As their name implies, tearing modes involve a reconnection of magnetic flux within the plasma and so are

limited in their growth rates to a resistive timescale. They can occur on any rational q flux surface, although they are most likely with low-order rational numbers, which minimizes the amount of energy-absorbing field line bending associated with the instability. Consequently the mode might have a number of causes, locations, or effects and occur at a range of β's, making it a concern for the ITER baseline scenario.

Conversely, the pressure-driven kink is a laminar distortion of the plasma that can grow on a very fast timescale but can be impeded by an interaction of the mode with conducting plasma-facing components. It represents a fundamental ideal MHD limit to the plasma and so impacts operating regimes at the highest β_N values—the aforementioned advanced scenarios, which are more resilient to tearing modes due to the avoidance of low-order rational q surfaces and the existence of regions of reversed magnetic shear.

Tearing modes can develop for two principal reasons in modern-day tokamaks. They can either arise directly, due to some inherent instability in the plasma, such as that arising from strong current gradients in the core, or they can be driven by other perturbations, such as those arising from axisymmetries in the magnetic field of the device (termed *error fields*), or indeed in response to magnetic perturbations arising from other instabilities in the plasma. There is some overlap in these categories, with, for example, some instabilities initially being driven by perturbations from other natural instabilities such as sawteeth. In fact, for the ITER baseline scenario, the principal concern for high performance arises from this type of process, with the sawtooth instability coupling to resonant surfaces farther out and giving rise to a neoclassical tearing mode (NTM). With this instability, once the initial island is triggered, the perturbation it then generates in the bootstrap current leads to strong drive for further growth, resulting in a much larger island that degrades performance.

The triggering of an NTM is a complex process. Not only does the threshold for NTM excitation involve several subtle mechanisms governing the evolution of a neoclassical island, but there also remain critical uncertainties in both the form and the controllability of the triggering instability and in the coupling process by which the triggering instability induces an initial island that grows to become the NTM. Nevertheless, in recent years there has been considerable progress both in understanding the mechanisms and developing control over them.

For ITER, NTM triggering remains a crucial issue since the mode is expected to account for the main β limit (here, β is the ratio of kinetic to magnetic pressure) in both H-mode[16] and hybrid scenarios.[17–19] The most serious concern is for the sawtoothing ELMy H-modes (the ITER baseline scenario), where the strong fast-particle populations from neutral beams with negative ion sources and fusion-born α particles are expected to partially stabilize sawteeth,[9] leading to long-period, large free-

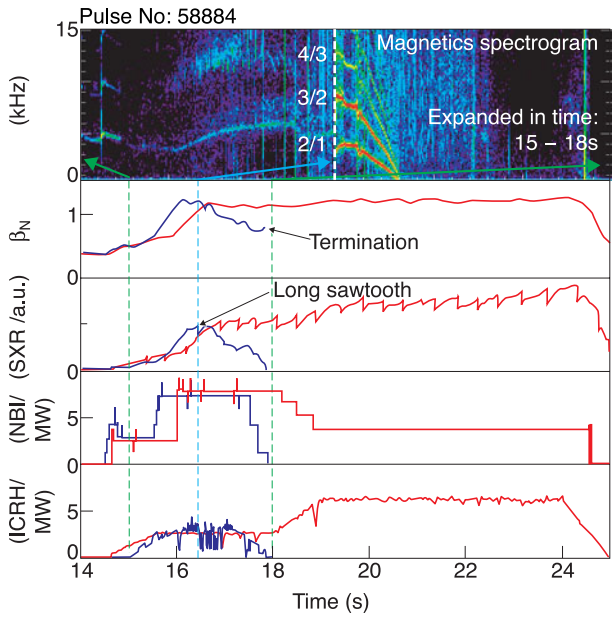

Fig. 1. Multiple NTMs excited by a long-period sawtooth crash at low β_N (pulse 58884 in blue/dark gray) and in a no-NTM case (pulse 58893 in red/light gray) obtained by carefully modifying heating timing and ICRH phasing in JET. From top to bottom: magnetic spectrogram (zoomed time range), β_N, core soft X-ray amplitude, neutral beam heating, and ICRH power. From Ref. 20.

energy events. As seen on JET (Fig. 1), such events can excite multiple types of NTM, and do so readily at low β_N values[20] ($\sim$1), leading to large falls in particle and energy confinement. Thus, issues that must be addressed for ITER and future tokamak fusion reactors include predicting and controlling the NTM thresholds, understanding consequences of the modes, and the requirements for NTM control or removal.

As mentioned, tearing modes can also be driven by asymmetries in the tokamak's magnetic field, termed *error fields*. During the past decade there has been significant progress on JET in the areas of error field–driven locked modes. Early in JET's life the phenomenon of locked modes, long-wavelength plasma instabilities that do not rotate in the laboratory frame, was identified as a major issue.[21,22] These locked modes frequently preceded disruptions[4] and were explained as being due to large-amplitude plasma instabilities driving eddy currents in the surrounding vacuum vessel, which in turn applied a braking torque to the plasma,[23,24] although the ultimate locking of the instability in the laboratory frame is due to interactions with helical magnetic error fields.[25] These error fields arise from imperfections in the magnetic field coils, as well as from the necessarily nonaxisymmetric feeds to the coils. Subsequently, error fields were identified as a source of instability in their own right,[26,27] and this effect was studied on JET (Refs. 28 and 29).

These error field instability studies generally, though not exclusively, are performed in low-β ohmic plasmas, since the modes pose a concern for ITER in the low-density ohmic phase prior to H-mode access. Nevertheless, at higher β, as the ideal $n = 1$ kink mode pressure limit is reached, the plasma can become increasingly susceptible to error field–driven instabilities being destabilized, which through the resulting slowing of the plasma rotation may allow resistive wall modes (RWMs) to be destabilized as first observed in DIII-D (Ref. 30). Thus, the error field plays an intimate role in influencing the RWM stability, both in directly driving flux surface distortions and in slowing plasma rotation, which can reduce other dissipative stabilizing effects on the RWM.

In this chapter we describe these issues in three main sections, exploring first in Sec. II (authored by R. J. Buttery) the neoclassical tearing mode, the role of the sawtooth, and the extrapolation and control of these aspects. Then, in Sec. III (authored by T. C. Hender) we describe the issues surrounding error fields at low β and the work done to identify requirements for the ITER design from this perspective. Finally, in Sec. IV (authored by Hender) we discuss studies of RWMs performed on JET and the use of applied magnetic perturbations at high β to diagnose their physics. A summary is given in Sec. V.

II. RESOLVING NTM AND SAWTOOTH PHYSICS FOR ITER

NTMs are magnetic islands in the plasma that are driven to large amplitude by the absence of bootstrap current in the island core. This absence of bootstrap, due to good conduction and flattening of pressure within the island, gives a helical current perturbation that enhances the size of the island when it is located in a region of positive magnetic shear. Thus, NTMs typically occur at moderate to high β (to produce high bootstrap current) in baseline and hybrid scenario plasmas. In the sections that follow we give a brief introduction to the formalism governing NTM behavior and then explain how this manifests itself in the observed experimental behavior and leads to the various control tools and avoidance techniques developed at JET for these performance-limiting instabilities.

II.A. Formalism: NTM Physics Scalings

To understand how the various physical mechanisms combine to trigger an NTM, it is useful to consider the modified Rutherford equation,[31,32] which governs the evolution of an island of full width w and minor radius r, at given poloidal beta β_p, in terms of the classical tearing stability index Δ', bootstrap a_{bs}, field curvature a_{GGJ}, ion polarization current a_{pol}, and finite island transport terms w_d:

$$\frac{\tau_r}{r}\frac{dw}{dt} = r(\Delta' - \alpha w) + r\beta_p\left[a_{bs}\left(\frac{0.65w}{w^2 + w_d^2} + \frac{0.35w}{w^2 + 28w_b^2}\right) - \frac{a_{GGJ}}{\sqrt{w^2 + 0.2w_d^2}} - \frac{a_{pol}\,w}{w^4 + w_b^4}\right] . \quad (1)$$

Here, the NTM is driven by a helical hole in the bootstrap current[33] that develops about an island due to pressure flattening (the a_{bs} term); this is dependent on the local poloidal β, β_p (with a small correction for field curvature,[34] the a_{GGJ} term). Once triggered, islands rapidly grow (on a resistive timescale, τ_r) to a saturated size, which to first order depends on the ratio of the bootstrap term to the classical tearing stability index [the $r(\Delta' - \alpha w)$ term, where the α introduces an island size dependence leading to saturation.[35]] By definition of an NTM, the classical tearing stability Δ' is negative at the time of its onset. However, tearing modes can also be destabilized if the Δ' becomes positive—strictly speaking, one might not label these as NTMs, but nevertheless once they reach large enough island size, they can be amplified by the same bootstrap effects discussed above to further grow "neoclassically" if β is high enough.

With just the terms discussed so far, NTMs would grow from zero island widths in all discharges with positive shear at a rational safety factor (q) flux surface. However, the w_d, a_{pol}, and w_b terms change this to make the NTM stable at small island size, leading to the requirement of a seeding event to induce a large enough island for bootstrap-driven growth to take over. These small island terms are due to the effects of finite transport over the island[36] (w_d term), ion polarization currents[37] (a_{pol} term), and the loss of bootstrap as size approaches ion banana widths[38] (w_b term). They are important in both governing the thresholds for the modes and the requirements for NTM control systems. Most significantly, they lead to a dependence of the NTM threshold β on normalized poloidal Larmor radius ρ^*, which is expected to play a key role in the scaling of NTM physics toward ITER. They also lead to a metastability threshold for the mode—a β value below which the NTM is unconditionally stable because the bootstrap drive is not strong enough to overcome stabilizing Δ' and small island effects.

As an example, we consider the ion polarization current term, which can be characterized by[39]

$$a_{pol} \propto g(\nu, \varepsilon)(L_q/L_p)^2\rho_{i\theta}^2\,\Omega(\Omega - \omega_i^*)/\omega_e^{*2} , \quad (2)$$

where g is a function of normalized collisionality $\nu = \nu_i/\varepsilon\omega_e^*$, with $g = 1$ for $\nu \ll 1$ and $g = \varepsilon^{-3/2}$ for $\nu \gg 1$, ν_i is the ion collision frequency, ω_e^* (ω_i^*) is the electron (ion) diamagnetic frequency, and $\rho_{i\theta}$ is the poloidal ion Larmor radius, with all quantities taken at the relevant

resonant surface. The term arises because as an island travels through the plasma, the ions see the island's electrostatic effects averaged over their banana orbits, while electrons see a more localized effect due to their smaller Larmor radii. For small islands (provided they are significantly larger than the ion banana orbit width), this leads to a net current (the ion polarization current) that can be stabilizing to tearing modes. Thus, the term also depends on the natural island propagation frequency (Ω) in the zero radial electric field frame of reference,[39] which is hard to measure experimentally and hard to predict theoretically. However, assuming that the Ω term is constant and in the direction to give a positive (stabilizing) sign for a_{pol}, then folding Eq. (2) back into Eq. (1), neglecting w_d and w_b terms, and assuming a given seed island size $w = w_{seed}$, we can solve for marginal growth ($dw/dt = 0$) to give a threshold for NTM onset in β_p that scales with ρ^*:

$$\sqrt{\frac{L_q}{L_p}}\beta_{p\text{-}onset} = -r_s \Delta' \rho^*_{i\theta} \frac{w_{seed}/w_{pol}}{[1-(w_{pol}/w_{seed})^2]}\, g(\nu,\varepsilon) \ , \tag{3}$$

where $w^2_{pol} = a_{pol}/(a_{bs}\varepsilon^{1/2}L_q/L_p)$ and $\rho^*_{i\theta} = \rho_{i\theta}/r_s$. This shows that a key element introduced by the small-island terms is a link between the minimum β_p for NTM growth, $\beta_{p\text{-}onset}$, and the island size at NTM onset. When w_{seed} is small, very high β_p is required for neoclassical growth, but as the seed size increases, the $\beta_{p\text{-}onset}$ falls, reaching a minimum at $w_{seed} = \sqrt{3w_{pol}}$ for the ion polarization model. Thus, larger triggering events, such as large sawteeth, are likely to trigger NTMs at lower β.

A similar form can be obtained with the finite island transport model (w_d term), as discussed in Refs. 40 and 41, where the parameter w_d is governed by the ratio of perpendicular to parallel heat conductivities. This also generates a linear ρ^* dependence, no collisionality dependence, and credible critical island sizes, provided parallel heat conductivity in the island region is modified from the usual classical Spitzer formulation to allow for Landau damping effects at low collisionality,[36,42] which give rise to a limit in the heat flux around the island.

These equations indicate the main behaviors and physics contributions involved in NTM evolution. We now discuss how these aspects have been explored experimentally at JET.

II.B. Early JET Observations and Tests of NTM Physics

NTMs were originally identified experimentally on TFTR (Ref. 43) and have since been found on a range of devices. Their first observation on JET was reported in Ref. 44. The basic island structure was determined (Fig. 2), and key elements of "neoclassical behavior" were identified: the scaling of island size with β, scaling of onset β with ρ^*, and the mode's metastability. At medium β_N values 3/2 NTMs (denoted as *m/n* for the *poloidal/toroidal* mode number) were observed. Mode evolutions were found to be well modeled by evolving the modified Rutherford equation that governs NTM stability. The modes were found to limit performance at high β, when they became manifest in their more serious ($m = 2$) $n = 1$ form. Thus, JET has subsequently invested considerable efforts in understanding the physics, avoidance, and control of these NTMs.

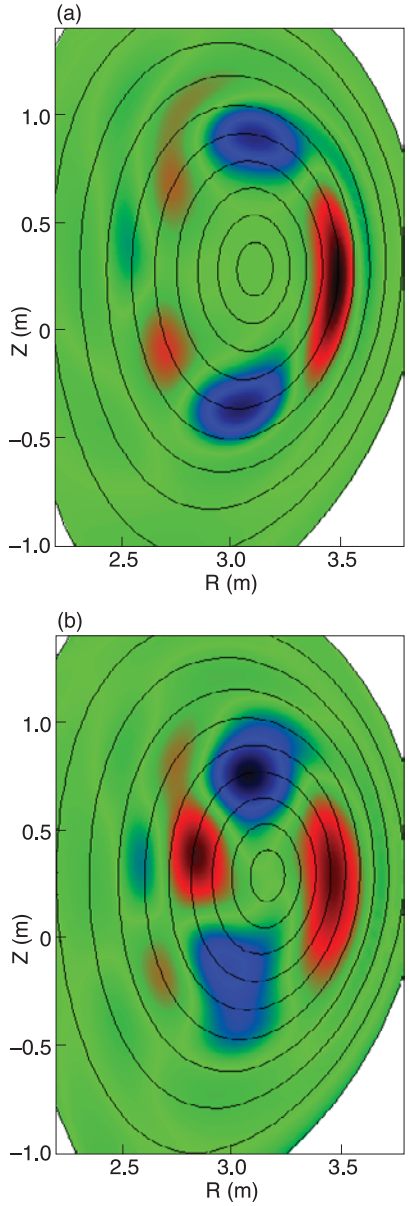

Fig. 2. NTM poloidal mode numbers identified by SXR tomography for cases at medium β_N (pulse 40563; $m = 3$, $n = 2$ mode) and high β_N (pulse 40564; $m = 2$, $n = 1$ mode). Color indicates deviation from equilibrium value on that surface (noting positive and negative deviations colored red and blue, respectively, which both show as dark gray shades in the print version). From Ref. 44.

The triggering and behavior of these modes was explored in further detail in Refs. 16, 45, and 46. Here, the deployment of controlled rampdowns in the heating power enabled the role of the small-island size effects to be elucidated. This confirmed a clear metastability β threshold, below which the 3/2 NTM self-stabilizes (Fig. 3). Such behavior was demonstrated to be consistent with either finite island transport effects or ion polarization currents giving rise to the small-island size stabilization effects. β threshold scalings for the mode were explored for a wide data set encompassing different JET machine geometries. These studies found the clearest correlations with the theoretically expected linear ρ^* dependence when comparisons were couched in terms of the appropriate NTM physics parameters, e.g., local thermal poloidal β rather than global total β_N (Ref. 46); it should be noted that most plots in this chapter are in the more noise resilient global β_N parameter, which gives a better understanding of operational limits and is a valid approach provided that key parameters such q_{95} and shape are held constant. The 3/2 NTMs were also found to have a significant effect on confinement (reducing it by typically ~15 to 20%), becoming disruptive and occurring with low-onset β_N as q_{95} was lowered below 3 (Ref. 16). Fast magnetic measurements confirmed the mode number inferred previously and identified a new 4/3 NTM, triggered at even lower β values. These measurements were also used to investigate the seeding process for the 3/2 NTM, which appeared to be associated with the sawtooth instability (to be discussed in Sec. II.E). Similarly, the β dependence of the 2/1 NTM island size was identified in (Ref. 29), in which mode excitations by large fast-particle-stabilized sawteeth and error fields were reported. Subsequent 2/1 NTM structure, triggering, and dimensionless parameter scaling were explored in Ref. 47.

II.C. Role of the Sawtooth in NTM Onset

The expectation of a ρ^* scaling discussed in Sec. II assumes that variations in the NTM physics terms in Eq. (1) dominate in the NTM onset process. However, considerable uncertainty exists in the mechanisms that lead to a seed island, and it can be speculated that as plasma heating is increased, these processes might change considerably. This was explored in Ref. 48, in which it was found (Fig. 4) that simple power law fits (in ρ^* and collisionality) to a data set of NTM onset β thresholds were not predictive of the β value at which the 3/2 NTM was triggered. Indeed, it is generally found that NTM onsets occurred along a trajectory in β versus ρ^* (Fig. 5) that aligns with a typical discharge's evolution. (From the definitions of β and ρ^*, one expects β to vary with

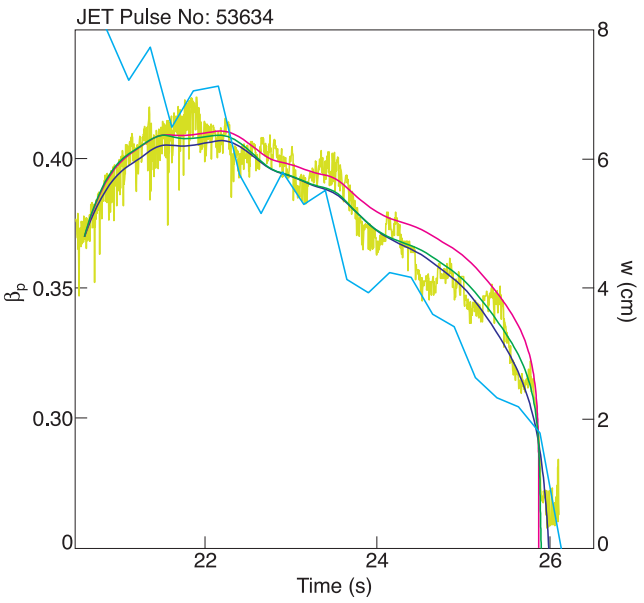

Fig. 3. Evolution of 3/2 NTM island size (noisy trace, right scale) during a β_p rampdown (jagged trace, left scale) for pulse 53634. Island size is compared with modeling using the modified Rutherford equation (smooth curves) with either the ion polarization current term (pink or medium gray) or the finite island transport term (blue or dark gray) or both (green or light gray) included. From Ref. 45.

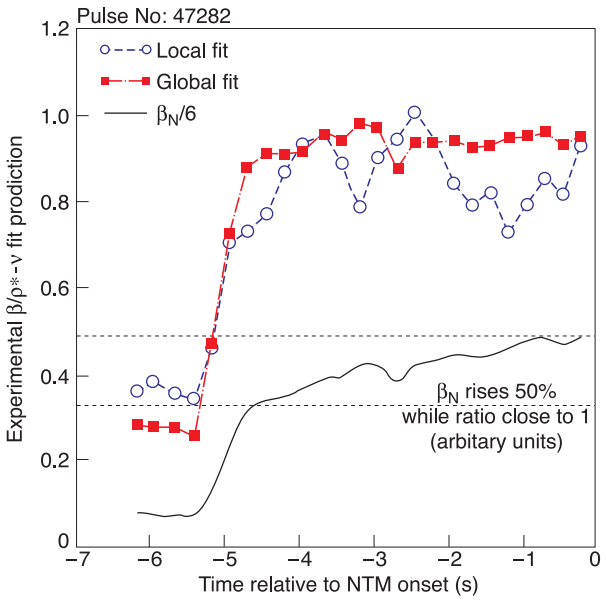

Fig. 4. Ratio of experimental β for pulse 47282 to the predicted 3/2 NTM onset β based on time-evolving ρ^* and collisionality values. The predicted onset β is taken from global volume average β_N values (squares) at time of NTM onset for a wide range of JET discharges, fitted to toroidal ρ^* and collisionality at time of NTM onset. The local fit (circles) is based on local poloidal thermal β values. From Ref. 48.

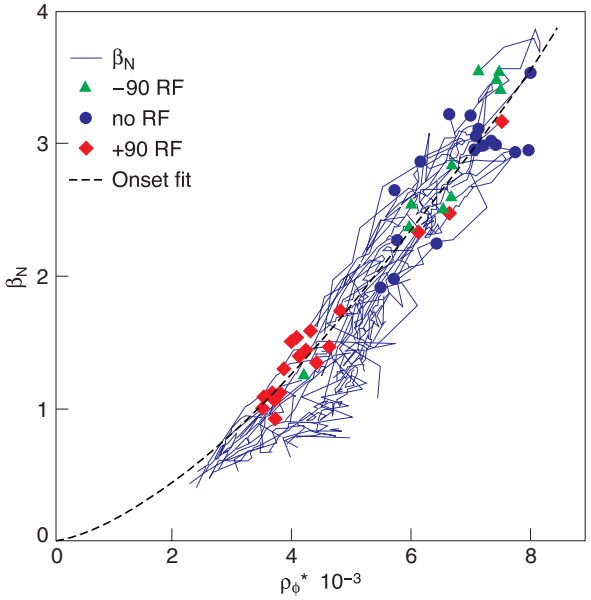

Fig. 5. 3/2 NTM onsets (symbols) and discharge trajectories (lines) for shots with and without ICRH. From Ref. 48.

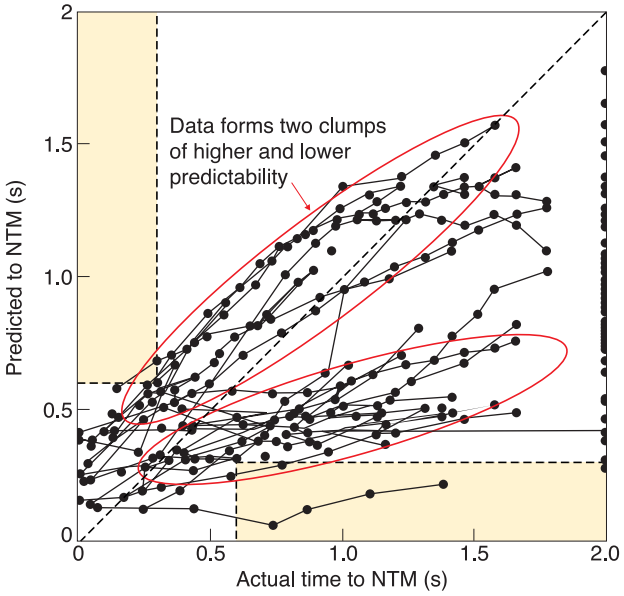

Fig. 6. Comparison of optimal neural network prediction of NTM onset time with actual time to NTM. From Ref. 48.

ρ^{*2} density; therefore, this near-linear β versus ρ^* evolution in each discharge indicates an underlying density—and possibly profile—variation as power is ramped up.) Thus, NTM onset is not simply a question of crossing some β limit as NTM physics terms evolve with heating power; the ρ^*-ν–based scalings of NTM onset, though well motivated physically, represent a necessary but not sufficient condition for NTM onset—additional physics mechanisms must be involved.

Neural network techniques were employed to explore a wide range of possible control parameters related to NTM onset. Interestingly, the optimum predictive performance was obtained with just three parameters: β_N, $\rho^*_{i\phi}$, and sawtooth period, as shown in Fig. 6. (Here, $\rho^*_{i\phi}$ is the toroidal ion Larmor radius normalized to the plasma minor radius.) Unlike simple ρ^*-ν–based NTM onset scalings, a neural network fed with these three parameters can clearly anticipate an approaching NTM. Discharges divide into two groups in Fig. 6: an upper group with onset during a rapid β rise and a lower group when discharges are evolving more slowly at high β. Predictability falls substantially if sawtooth period is removed from the network, while further tests showed that given a choice between sawtooth period and magnetic precursor size, the network finds period most significant. This is also observed phenomenologically,[13] with long sawteeth not having significantly larger magnetic precursors but clearly observed to trigger NTMs more readily. (Note that the network optimizes performance with β_N and $\rho^*_{i\phi}$, rather than the more physically motivated local β_p and $\rho^*_{i\theta}$ measurements, which because of the nature of their calculation introduce greater scatter in the data.) The role of the sawtooth is identified explicitly in Fig. 7, where the β dependence of NTM onset thresholds with sawtooth period indicates an apparent threshold in sawtooth period above which NTM onset can occur at low β_N, close to its β threshold for NTM metastability (below which the mode becomes unconditionally stable).

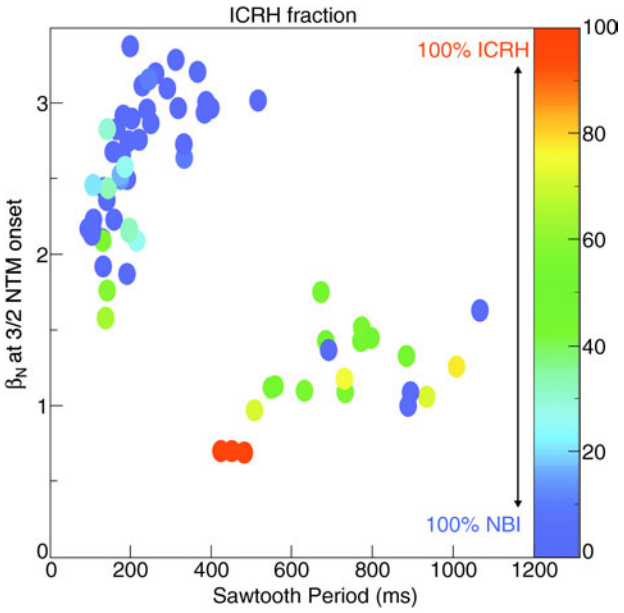

Fig. 7. Dependence of 3/2 NTM onset β_N on $\tau_{sawtooth}$ and heating mix in JET. From Ref. 48.

The role of sawtooth period raises an interesting question. References 13 and 48 showed that other measures of sawtooth precursor or crash amplitudes did not explain the data well. For sawteeth triggered before a crash, magnetic precursor amplitude did not play a strong role in setting the onset β (although the final timing of the NTM onset between the sawteeth correlated well with the time of peak magnetic amplitude, as described in Sec. II.E). For sawteeth triggered by the crash itself (e.g., in Ref. 13), the amplitude of soft X-ray (SXR) crash size or $n = 1$ magnetic signals associated with the sawtooth MHD were not found to correlate with NTM onset or indeed with sawtooth period—many signals of similar or larger amplitude were found before the NTM-triggering event. In Ref. 48 a range of further underlying parameters were also explored (including collisionality, $q = 1.5$ radius, safety factor scale length at $q = 1.5$, and internal inductance), none of which provided improved predictability of the NTM onset. The actual mechanism by which the NTM is triggered remains somewhat uncertain, from both experimental and theoretical perspectives, although it can be speculated that the role of the sawtooth period might be indicative of a buildup of free energy associated with current and pressure profile evolutions, leading to the potential for increased drive in the initial seed island formation. These seeding issues are considered further in Sec. II.E.

These results highlight the importance of considering and controlling the amplitude of the MHD that drives the initial formation of the seed island, which then grows to become an NTM. We now consider the application of this to the specific case of the fast-particle stabilized sawteeth that are likely to trigger NTMs in ITER's baseline scenario.

II.D. Prediction and Control of Sawteeth

In a burning plasma, it is expected that the strong energetic α population present will partially stabilize sawteeth, leading to large infrequent events that trigger the NTM at low β_N—an effect observed directly on JET with ICRH-accelerated ^{4}He ions.[11] The importance of sawtooth control is highlighted by recent experiments on JET. Here, it is found that low-β NTMs (e.g., short pulse with blue/dark curves in Fig. 1) could be avoided by utilizing two strategies: First, ICRH phasing was switched to one that reduced the core particle pinch (from dipole phasing to -90 deg). Second, the timing of the heating power rise was delayed to establish a sawtoothing auxiliary heated L-mode, prior to H-mode entry. This is conjectured to reduce profile peaking and magnetic free energy in the core before the introduction of strong fast-particle populations and thereby avoid a long first sawtooth that triggers the NTM. This led to dramatically reduced mode activity with improved performance and stable operation at much higher input power, as shown in the longer surviving pulse in Fig. 1. Thus, careful consideration of plasma profiles and operational development can avoid the most severe effects of NTMs.

For sawteeth in ITER and burning devices, two strategies are possible:

1. strong sawtooth stabilization with early α production if possible
2. sawtooth destabilization to make them small and benign.

Latest estimates[49] suggest that the former can delay the first sawtooth for perhaps 50s in ITER, allowing thermal equilibration. Significant extensions may be possible with extensive use of current drive techniques[50] or modifications to the start-up, but these will change the scenario behavior and performance and are still likely to be pulse length limited, hindering the ability to explore long-pulse evolution or execute materials testing. Sawtooth destabilization was demonstrated on JET using ion cyclotron current drive (ICCD) in the 1990s to modify $q = 1$ shear[12] and in 2000 to raise NTM thresholds.[13] However, these results were obtained in regimes without significant fast particles, where the sawtooth crash occurs when the most unstable *resistive* internal kink exceeds diamagnetic frequencies, yielding a criterion in terms of local shear.[51] For the (partially) fast-particle-stabilized sawteeth expected in ITER, the trigger for instability can still be formulated in terms of a criterion in the shear at $q = 1$, but the threshold shear is proportional to the potential energy of the *ideal* internal kink mode, which increases as a result of fast ions in the core. It was unclear theoretically whether localized current drive could be sufficient to overcome the stability threshold in this new situation where the stability is enhanced by the presence of energetic ions.

This question was answered by new experiments on JET using two types of ICCD (Refs. 14, 52, and 53): one to first establish a strong-core fast-particle population and large sawteeth (dashed lines in the third and fourth panels of Fig. 8) and the other to drive localized current at the $q = 1$ surface (solid lines). It was found that as the current drive location (solid line, third panel) approached the sawtooth inversion radius (dotted trace in third panel), the sawtooth period (second panel) and amplitude (first panel) fell dramatically. Conversely, with other ICCD phasings or deposition locations, the sawteeth were not destabilized, demonstrating that the effect is due to localized current drive. These results put sawtooth destabilization in ITER on a much firmer footing. They are complemented by progress on other devices using electron cyclotron current drive (ECCD), the likely tool for localized current drive in ITER. An important further step to take will be to employ a population of ICRH in the core region to stabilize the sawteeth and apply ECCD near the $q = 1$ surface to destabilize the sawteeth. This procedure will differ from the dual-resonance ICRH procedure outlined above in JET because the threshold shear

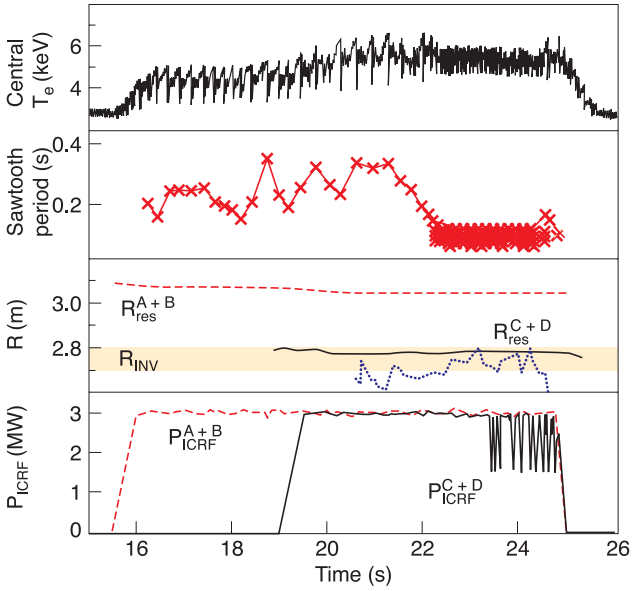

Fig. 8. Effect of $q = 1$ current drive on ICRH-stabilized sawteeth in JET pulse 58934. Sawtooth amplitude (top panel) and period (second panel) increase with application of core-resonant ICRH (dashed line, third and fourth panels, indicating resonant location and heating power). When ICRH current drive in the vicinity of $q = 1$ is added (solid line), this has a destabilizing effect on sawteeth as the resonance location aligns with the sawtooth inversion radius (dotted trace, third panel). From Ref. 52.

for instability (governed by the fast ion pressure gradient) will not be significantly modified by the $q = 1$ resonant population when ECCD is used.

For ITER, there are additional concerns, and opportunities, arising from the highly energetic (~1 MeV) negative ion neutral beams (NNB). These can also stabilize the sawteeth (e.g., on JT-60U, Ref. 54), as explained in Ref. 55, due to finite orbit effects from ions intersecting the $q = 1$ surface, changing the free energy available to drive the instability. However, with suitable deposition (e.g., outside $q = 1$), the NNB can also be destabilizing to make smaller frequent sawteeth.

A further effect is associated with strong neutral beam momentum injection, due to stabilizing kinetic effects at high plasma rotation. Although this is not likely to be a factor in ITER, it is vital to take account of this in modeling present devices, since it can lead to substantially longer sawtooth periods. This has recently been measured on JET (Ref. 56; Fig. 9a), with results showing qualitative consistency with earlier predictions[57] of the critical β_p for triggering a sawtooth (Fig. 9b). More recently, specific modeling for these experiments has shown good agreement with the experimental trends.[58,59]

The effects of fast particles and other parameters on sawtooth and NTM stability highlights the need for practical sawtooth destabilization tools to be developed. Work is needed to demonstrate the control techniques that JET has pioneered, using localized current drive systems in high fast-particle content, baseline scenario–type plasmas at high β.

II.E. The NTM Seeding Process

The other element that is central to the understanding and prediction of NTM onset is the seeding process by which an MHD event triggers an NTM. There are a range of possible mechanisms that can apply, as might be expected from the observation of the low metastability threshold for NTMs in present devices. It is important to explore and resolve these for ITER. We start by considering the 3/2 NTM, which is particularly susceptible to core instabilities such as the sawtooth.

Early NTM seeding models focused on the possibility of magnetic coupling between some MHD event (such as a sawtooth precursor) and the NTM resonant surface, exciting an island that would then grow neoclassically.[60]

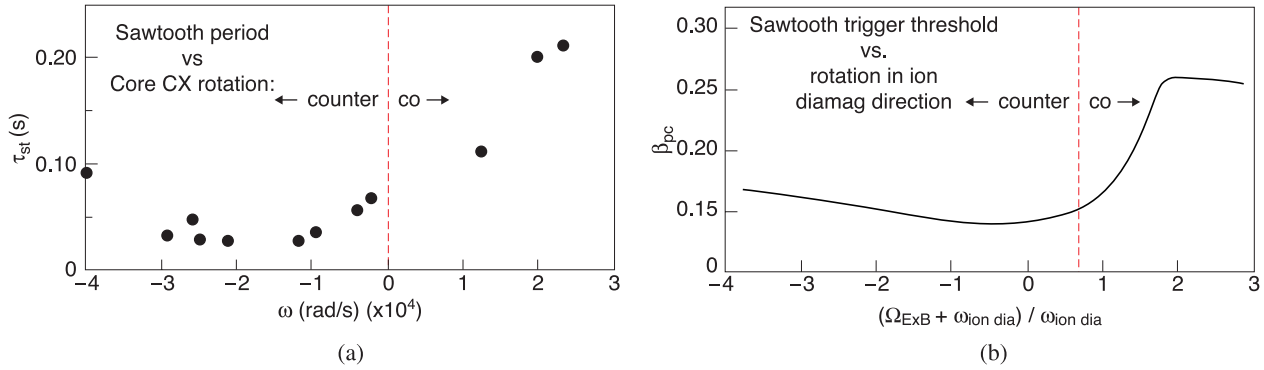

Fig. 9. (a) Sawtooth period versus plasma rotation for neutral beam coinjection and counterinjection at various power levels on JET. (b) Critical β_p for ideal internal kink as a function of normalized plasma rotation.

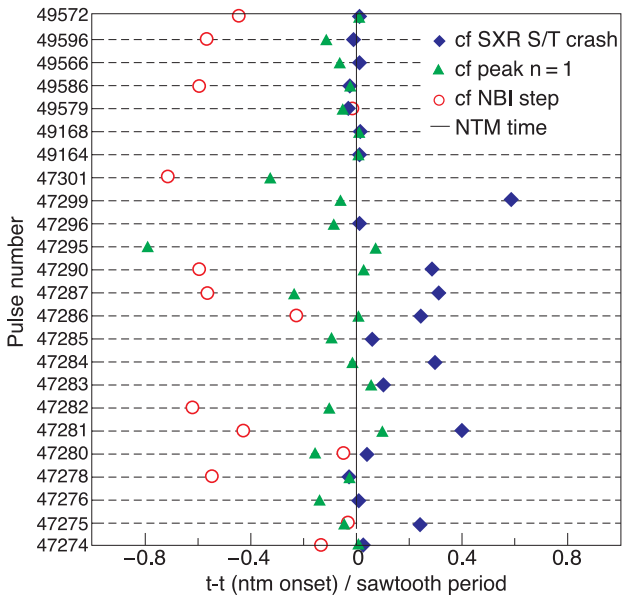

Fig. 10. Correlation of NTM onset time ($x = 0$) with sawtooth crash (diamonds) and precursor peak magnetic amplitude (triangles). From Ref. 46.

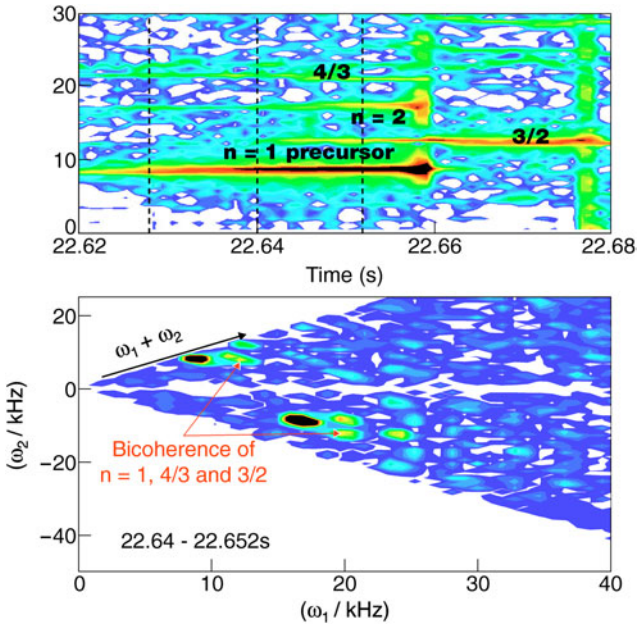

Fig. 11. Spectrogram (top) and bicoherence plot (bottom) for JET pulse 51995. The bicoherence plot indicates the degree of coherence between a beat wave arising from modes at ω_1 (x axis) and ω_2 (y axis) and a third mode at frequency $\omega_1 + \omega_2$. This shows that the $n = 1$ sawtooth precursor and 4/3 mode combine to make a signal with a high degree of phase coherence with the 3/2 mode (arrowed points). Other points arise from elements such as coherence between $n = 1$ and $n = 2$ sawtooth precursor harmonics. From Ref. 20.

Indeed, 3/2 NTMs are often triggered during extended phases of sawtooth precursor activity, and usually near the peak of the magnetic perturbation[46] (Fig. 10). The mode frequencies generally preclude direct toroidal coupling of the 3/2 NTM to the nonlinear $n = 2$ harmonic of the sawtooth precursors, but a further possibility[61] lies in "three-wave" coupling, whereby magnetic perturbation due to the 1/1 sawtooth precursor and the 4/3 NTM combine to induce a beat wave perturbation with $m = 3$, $n = 2$ structure. Here, the $q = 1$, 4/3, and 3/2 resonant surface rotation frequencies are generally better matched to facilitate this process with $\omega_{q=4/3} - \omega_{q=1}$ close to $\omega_{q=3/2}$. Indeed, such coupling is highlighted in some cases by bicoherence analyses of JET data showing clear phase locking between driving (4/3 and 1/1) and driven (3/2) perturbations (Fig. 11). However, such frequency matches are not generally established, or correlated with NTM growth, indicating the need for further investigation.

A further mechanism has been proposed to explain magnetic triggering of NTMs, based on the transient changes to the transport properties around a magnetic island resulting from an MHD event.[62] The model relies on the existence of neoclassical ion polarization currents [see Eq. (2)], whose stability properties depend on the island rotation frequency in the $E \times B$ rest frame. The theory accounts for the competing dissipative mechanisms that influence the island rotation. An MHD event can transiently increase the electron dissipation and cause the island to rotate in the electron diamagnetic direction. This affects the sign and amplitude of the neoclassical ion polarization currents that influence nonlinear evolution as described by a_{pol} in Eqs. (1) and (2). Hence, MHD events may transiently eliminate or reverse the ion polarization threshold mechanism and lead to island growth. This theory may explain instances on JET when NTM growth correlates with sawtooth precursor activity but occurs without the frequency matching required for direct mode coupling.[45]

In hybrid scenario plasmas spontaneous (and fairly benign) 3/2 tearing modes are also sometimes found to occur,[63] although these are considered to be classically tearing driven, due to modifications of the current profile with lower hybrid current drive. Similarly spontaneous 2/1 classical tearing modes can be destabilized in this regime by excessive current drive.[64] Such modes can be avoided by reducing lower hybrid preheating of the plasma.

We now turn to the 2/1 NTM, which has the most serious impact on performance in tokamak plasmas. These generally occur above 3/2 NTM β thresholds, although with large sawteeth the chances of obtaining a 2/1 NTM are greatly increased (as in Fig. 1). At high β_N, 2/1 NTMs can be triggered by sawteeth or edge-localized modes (ELMs), especially at lower q_{95}, but do not always require a triggering instability.[47] Although β thresholds

align to a ρ^* scaling, modes most commonly occur close to the with-wall β limit. This has driven the adoption of a theory based on poles in the classical tearing stability, Δ', which develop as ideal limits are approached. This model was applied to DIII-D (Refs. 65 and 66), where it was found that Δ' slowly evolves toward instability as β_N rises toward the ideal β limit. Thus, these "triggerless" instabilities are likely to arise as classical (Δ' driven) tearing modes, but once their width becomes large enough, they are then driven further to large amplitude by neoclassical bootstrap effects. The implication of this interpretation may mean that the ρ^* scaling observed so far may not extend to medium or low β_N—an area now being further tested on JET with increased heating power.

A further influence on 2/1 NTM thresholds originates from error fields, which naturally arise in tokamaks due to asymmetries required in the design (e.g., coil current feeds). The influence of these error fields can be studied by deliberately applying further field perturbations using additional magnetic coils installed for this purpose (described in Sec. III). On JET, error fields were found to lower 2/1 NTM β_N thresholds by up to ~35% and caused the modes to form in the much more dangerous locked mode state (Fig. 12; Ref. 67). This indicates that error field and neoclassical drives for island growth can combine, with increased error field sensitivity (and plasma braking) at high β_N. The mechanism for this combination of drives is not well understood in JET—it could be related to changes in the underlying neoclassical tearing stability, for example, through ion polarization currents responding to changes in rotation in the $E \times B$ frame. Alternatively, error fields might act more directly, providing a small seed island to trigger NTM growth. As discussed in Secs. III and IV, such a process might be enhanced by the increased error field sensitivity plasmas exhibit at high β_N. However, a study in JET-matched experiments on DIII-D found a similar effect but with the initial mode formed rotating. Also, the rotation rate of the mode relative to background plasma varied with the degree of error field. This suggests that error fields can act at least in part through changes to the NTM stability, rather than by directly driving locked modes.

Fishbones are also found to trigger NTMs. Early results from ASDEX Upgrade[68] showed 3/2 NTM onset β versus ρ^* scalings to be ~20% higher in β when they are triggered with fishbones instead of sawteeth. However, JET data (Fig. 13) showed that such fishbone-triggered NTMs are limited to high β_N values, >2.5, but otherwise follow the same trend as the sawtooth-seeded cases, when plotted both in terms of β_N (shown) or in β_p. Fishbones have also been observed to trigger 2/1 NTMs at high β_N (~2.5) in JET hybrid scenarios,[20] where the modes can then limit β. The key to avoiding these events is to operate with increased central safety factor, well above unity, or to allow 3/2 NTMs to grow, which appear to remove some of the drive for the fishbone.

II.F. Impact of the Mode and Scaling and Implications for ITER

With a range of seeding mechanisms, the underlying criteria for neoclassical growth becomes crucial, the key

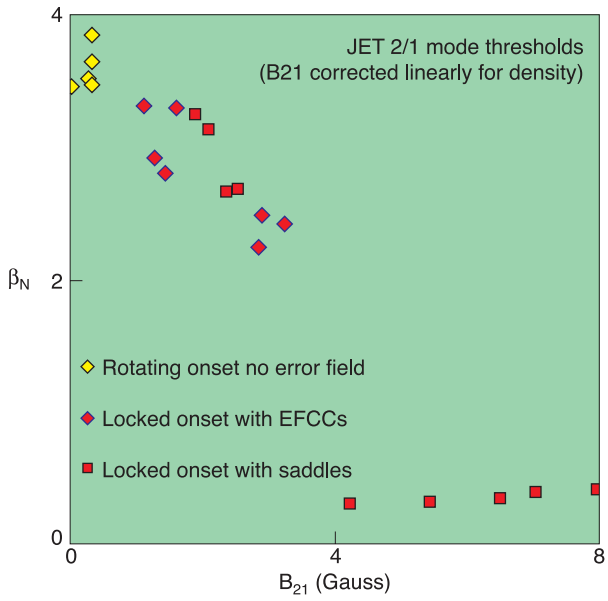

Fig. 12. Effect of applied error field on tearing mode threshold on JET. Error field applied by JET's internal saddle coils (squares) or external EFCCs (diamonds). From Ref. 67.

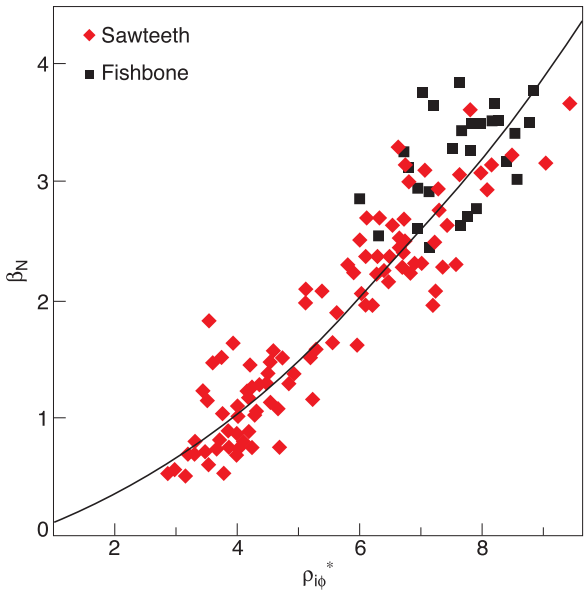

Fig. 13. Fishbone- and sawtooth-seeded 3/2 NTM onset β_N in JET. From Ref. 20.

question being, how do the stabilizing small-island terms scale toward ITER? These govern not only the sensitivity to triggering events but also the requirements for control of small islands and their removal by electron cyclotron systems in ITER. Previous studies[16] have shown a clear ρ^* dependence in the onset β for 3/2 and 2/1 NTMs on present devices. If unchecked, this would extrapolate to very low NTM β thresholds in ITER. To understand whether this trend will be borne out requires a detailed understanding and measurement of the underlying physics.

By performing β rampdown experiments and fitting consequent island size evolutions using Eq. (1), as in Fig. 3, it is possible to empirically measure the size and scaling of these small-island effects, allowing direct extrapolation to ITER. Cross-machine experiments have been executed on JET, DIII-D, and ASDEX Upgrade to address this for the 3/2 NTM. Results show a clear trend, with the metastability β threshold (Fig. 14, plotted in terms of local parameters related to the underlying NTM bootstrap drive) falling with normalized poloidal ρ^*. Preliminary analysis also suggests that the sizes of the small-island stabilization terms do not vary substantially with $\rho^*_{i\theta}$. This suggests a challenging task for ITER, to operate well above the metastability threshold; complete NTM removal would require modulated ECCD to drive island sizes down to levels similar in absolute value to those required in present devices.[69] Similar work is continuing for the 2/1 NTM.

With the likelihood of a range of types of NTMs in ITER, it is important also to understand their impact on the plasma—which modes are likely to be a problem. The 2/1 NTMs clearly have the most serious impact (e.g., Fig. 1), triggering ~50% confinement falls, transition to L-mode and disruptions. They are clearly unacceptable in ITER (Ref. 16). However, 3/2 NTMs are also significant (with ~15 to 20% confinement falls) and could impact fusion power substantially.[16] Their effects have been explored further in JET trace tritium experiments, using horizontal and vertical neutron cameras to track the progress of a tritium puff, constraining transport simulations. Preliminary results show that the 3/2 NTM is consistent with an ~50% reduction in the inward pinch in the vicinity of the island,[70] thus explaining the decreased particle confinement and density fall frequently observed with NTM onset.

Recent work has also shown that at low q_{95}, even higher harmonic NTMs can have a significant effect. For example, in JET shot 62129 (Fig. 15; 3.7 MA, 2.9 T, and $q_{95} = 2.7$), successively higher number modes are associated with steps in confinement and neutron rate. With the 4/3 NTM present, neutron rates are ~30% lower than values once all the modes have disappeared, while stored energy is ~13% lower. Although there is a slight evolution in the current profile (linked with and probably accounting for the appearance and decay of each mode), the ELMs, heating power, and plasma density remain constant in this pulse. Thus, it seems likely that the high m/n modes are accounting for most of this behavior.

With respect to the 3/2 NTM, some encouraging results have been reported at higher β_N (>2.3). Here, a nonlinear three-wave interaction with an ideal 4/3 mode and the 1/1 sawtooth precursor leads to sharp reductions in 3/2 NTM amplitude[71] (Fig. 16) and consequent confinement recovery. These are called FIR-NTMs

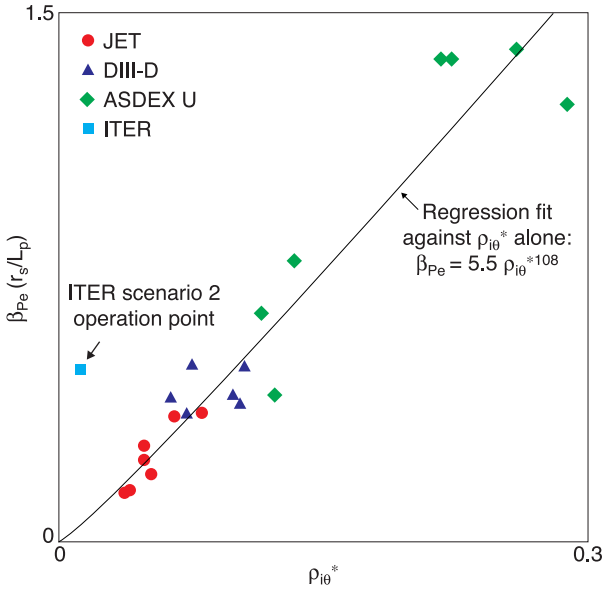

Fig. 14. 3/2 NTM metastability threshold scaling plotted against normalized poloidal ion Larmor radius, together with ITER's baseline operational point. From Ref. 20.

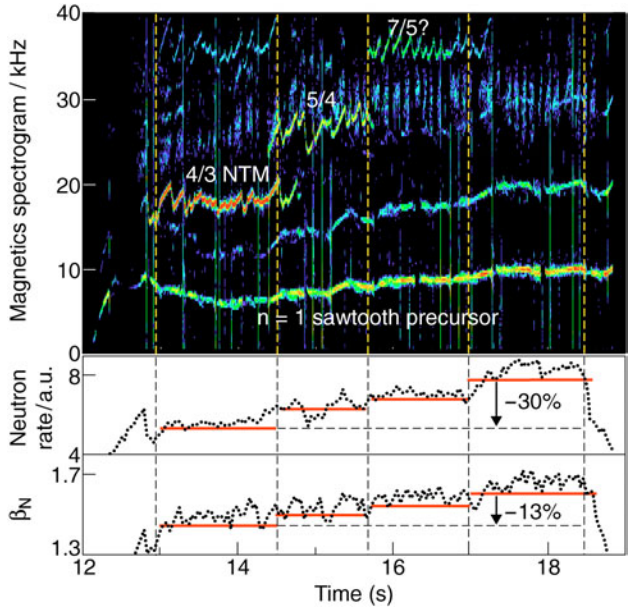

Fig. 15. Evolution of discharge with modes at constant heating power in JET pulse 62129. From Ref. 20.

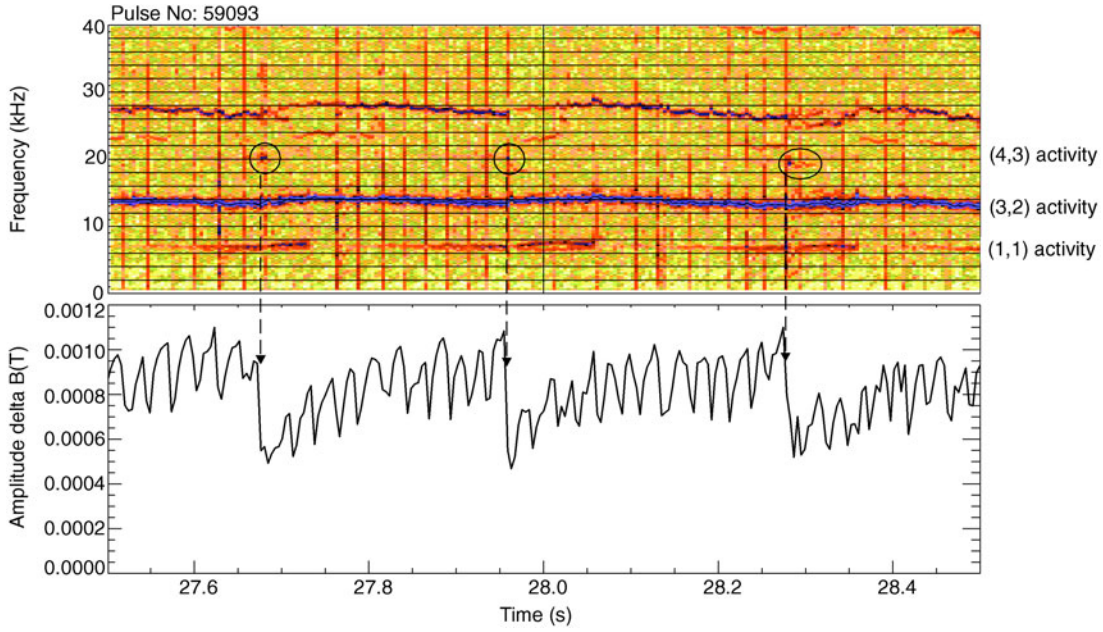

Fig. 16. Wavelet magnetics plot of FIR 3/2 NTM suppression (top). The 3/2 mode amplitude (lower panel) is reduced when bursts of 4/3 activity (circled in upper panel) couple to 1/1 sawtooth precursors, provided the 4/3 and 1/1 frequencies are consistent with three-wave coupling to 3/2 frequency. From Ref. 71.

(frequently interrupted regime) and were first identified on the ASDEX Upgrade tokamak.[72] These studies have also shown how this regime can be stimulated more readily using lower hybrid current drive to reduce shear at $q = 4/3$ and trigger the 4/3 mode. This may be a useful development for high-β operation such as for some variants of the hybrid scenario.

Turning to ITER implications, we see that a range of NTMs and triggering mechanisms pose a concern. But we also see that the problem is becoming tractable, with benign scalings for some events (such as the ideal β_N limit that may govern the 2/1 NTM onset) and the possibility of control when scalings are adverse (for example, of the sawtooth). In baseline scenarios the most serious limit originates from sawteeth, where there is good progress in predicting and controlling behavior. Further triggers (fishbones, Δ' poles, and possibly ELMs) occur at higher β_N, but it seems at least possible that these will be at similar β_N in ITER. In the hybrid scenario, the main concern remains the 2/1 NTM at high β_N—even though most of the seeding mechanisms prevalent in the baseline scenario have been removed. The extrapolation of the hybrid scenario 2/1 NTM β limit needs to be tested, although the "delta prime" theory of seeding close to the ideal β limit is encouraging in that limits in ITER may not be much lower than on present devices. However, with theory predicting greatly increased sensitivity to NTMs in ITER, due to its low ρ^*, we must not be complacent. There remain many aspects that need further theoretical and experimental elucidation, not least the seeding, while the strong α and NNB fast particle populations will make sawtooth control challenging. So, although the principal physics ingredients have now been identified, work needs to focus on measuring and explaining events in detail in order to predict behavior and requirements for ITER. And control techniques must also be developed as robust, ready-to-use tools, rather than lengthy research programs for ITER. In particular, the most promising techniques utilize ECCD, and this is likely to be needed. Studies on JET must explore the underlying physics to specify the requirements for this system, and if possible such a system should be implemented at JET to study the NTM stabilization process in conditions closest to those of ITER.

III. ERROR FIELD LOCKED MODE STUDIES

III.A. Scaling Studies

Error field locked modes are understood to arise from the braking torque applied to the plasma from a static error field, which can bring the rotating plasma to rest (most notably at $q = 2$) and allow islands to form (again, most notably those with poloidal and toroidal mode numbers of $m = 2$ and $n = 1$, respectively). Initial studies in this area were conducted on the COMPASS tokamak[27,73] complemented by theory development,[26] and showed an approximately linear dependence on the amplitude of the error field required to induce a locked mode with plasma density. The various dependencies of the error field B_{pen}

needed to cause mode penetration (i.e., induce a locked mode) were parameterized by an empirical scaling in the 1999 ITER Physics Basis[74]:

$$B_{pen}/B_T \propto n^{\alpha_n} B_T^{\alpha_B} q_{95}^{\alpha_q} R^{\alpha_R} \quad , \tag{4}$$

where B_T is the vacuum toroidal magnetic field, n the plasma density, q_{95} the safety factor at the 95% flux surface, and R the major radius. Studies on JET (Ref. 29) were important in establishing the various α scaling coefficients in Eq. (4). In cross machine scaling comparisons,[75] tokamaks with nearly the same aspect ratio were compared, so Eq. (4) does not contain an aspect ratio–dependent term. These error field mode locking experiments are conducted using nonaxisymmetric coils to deliberately apply error fields. Until 2003 these error fields in JET were applied using four saddle coils within the lower part of the vacuum vessel (Fig. 17a). Toroidally opposite coils were connected in antiseries so that only odd-n and dominantly $n = 1$ fields were applied. These two pairs of series-connected coils were powered from two separate amplifiers, allowing the phase of the applied $n = 1$ field to be varied. From 2003 error fields have been applied using large error field correction coils (EFCCs) external to the vacuum vessel (Fig. 17b), and during a shutdown in 2004 and 2005 the internal error field coils were disabled.

For ITER a key point at which locked modes may be induced is during the low-density ohmic phase, with the low density being needed to lower the H-mode threshold power requirement. Hence, for error field–driven locked modes, ohmic studies are particularly important. For ohmic plasmas α_R can be determined from the ohmic scale-invariance constraint,[76] $8\alpha_n + 5\alpha_B - 4\alpha_R = 0$ (which applies equally to the nondimensional locked mode threshold B_{pen}/B_T as to the context of normalized energy confinement in which it is derived in Ref. 76). A typical error field experiment pulse from JET is shown in Fig. 18 for a single-null divertor plasma [with I_p (MA) = B_T (T) = 2.5, elongation = 1.6, and $q_{95} = 3.4$]. In this case the field from the internal saddle coils (Fig. 17a) is ramped until a nonlinear response is seen in the locked mode detectors (a combination of coils measuring predominantly $n = 1$ radial field), indicating formation of an island in the plasma, or "penetration" of the applied field. Electron cyclotron emission measurements also indicated a flattening in the temperature profile at the expected location of the $q = 2$ surface and locked mode detectors identify the mode as $n = 1$, confirming the mode as a (2,1) island.[29]

Experiments of this type on JET showed a linear dependence of the error field penetration threshold on density (Fig. 19). In these experiments the intrinsic error field inherent in the machine has to be determined. This is done by applying the four quadrature phases from the error field coils (in this case the internal coils, Fig. 17a); for otherwise identical discharges the observed variation in error field threshold is due to the intrinsic error enhancing (or reducing) the natural error. For the 2.5-MA discharge used in these JET experiments (Fig. 18), the intrinsic error field normal to the equilibrium flux surfaces is equivalent to 1.2 G of $m = 2$, $n = 1$ radial field at the $q = 2$ surface (here, the Fourier analysis is performed in straight field line coordinates).

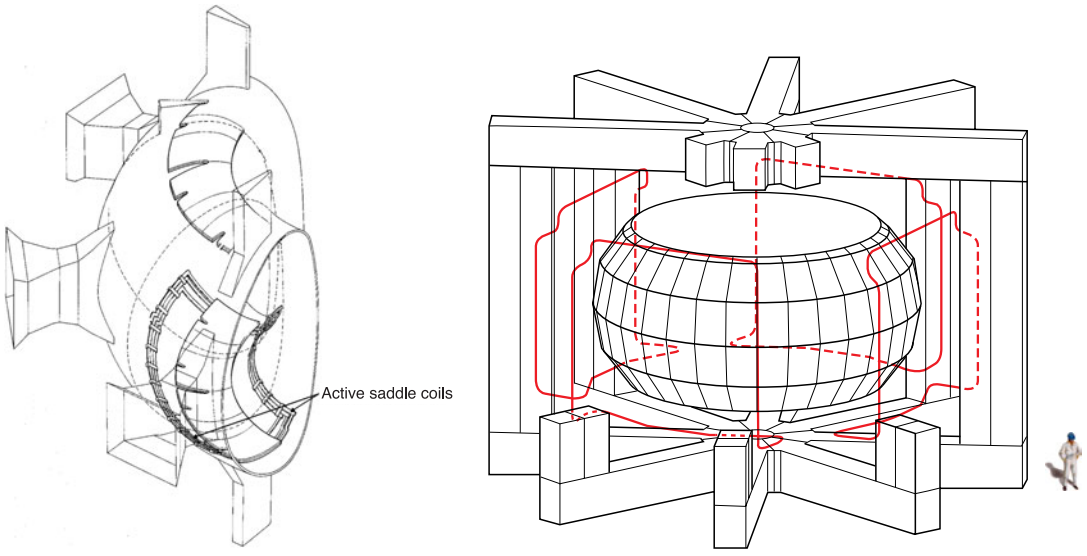

Fig. 17. (a) One-quarter toroidal section of JET showing the active internal saddle coils used for error field experiments until 2003. (b) Perspective view of JET showing the four large EFCCs that run between the transformer limbs. These coils have been used for error field experiments since 2003.

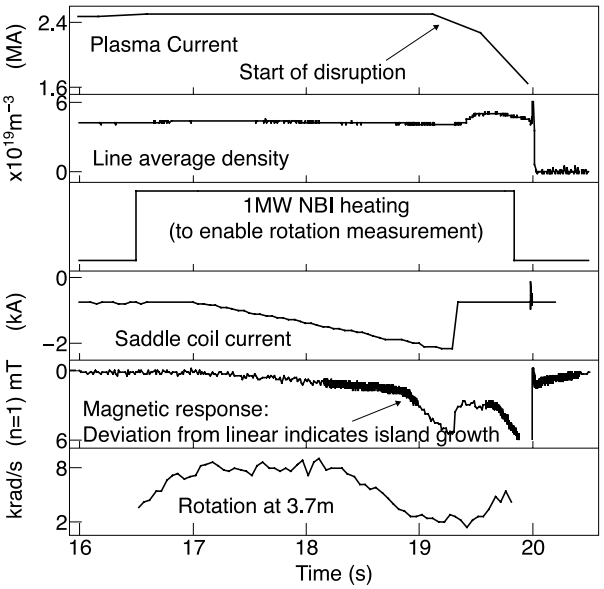

Fig. 18. A typical low-β locked mode pulse (44164). The saddle coil current is increased until a locked mode is destabilized, as indicated by the deviation of measured $n = 1$ radial magnetic field from a linear response. The rotation at $q = 2$ (measured by a charge exchange on carbon ions) can be seen to brake as the locked mode forms. In this case the residual locked mode induces a disruption—this is not always the case. From Ref. 29.

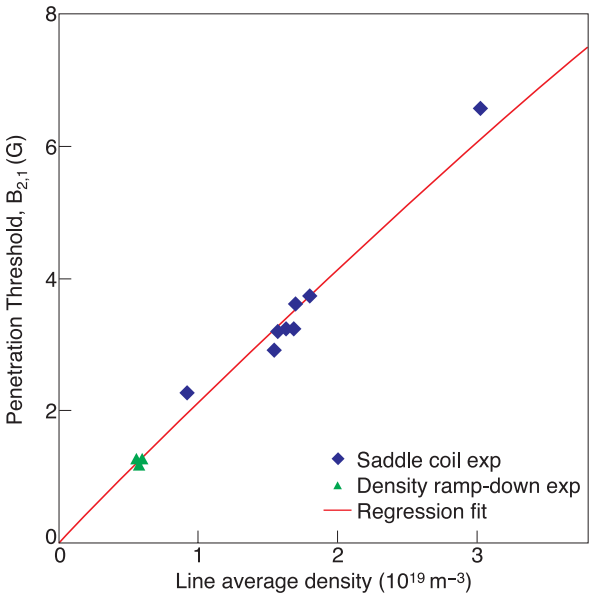

Fig. 19. Density scaling of error field penetration threshold, quantified in terms of the total (intrinsic + applied) $m = 2$, $n = 1$ field normal to the equilibrium flux surfaces at $q = 2$. Data from experiments with no applied field (triangles), where the density is ramped down to determine the intrinsic error field threshold, are included.[29]

Least-squares regression fits to scaling experiments show $\alpha_n = 0.94$, $\alpha_B = -1.2$, and $\alpha_q = 0.05$. These scalings are for the internal saddle coils (Fig. 17a); the scalings have also been checked with the EFCCs (Ref. 77). It is found that the scalings with density and toroidal field are essentially unchanged but that with the EFCCs, $\alpha_q = 1.65$; this large variation in α_q is thought to be because as q_{95} is varied, the effects of the error field sidebands (notably $m = 1$ and 3, $n = 1$) change, and so the differing spectral contents of the internal and external coils affects the q_{95} scaling.

A key feature of the JET results was the toroidal field scaling ($\alpha_B = -1.2$), which was substantially weaker than the corresponding result from COMPASS-D, $\alpha_B = -2.9$, but close to the DIII-D result, $\alpha_B = -0.96$ (Ref. 74). Confirmation of a weaker dependence on the toroidal field is optimiztic in terms of predicting error field thresholds in higher-field machines such as ITER. The scale invariance requirement, $8\alpha_n + 5\alpha_B - 4\alpha_R = 0$, predicts from the JET results that $\alpha_R = 0.4 \pm 0.2$. Using this value, the JET results predict an error field threshold for the 1998 ITER reference parameters (see Chap. 1 of Ref. 74) of $B_{2,1}/B_T$ of 1.25×10^{-4}, a value that is well within the capabilities of the proposed ITER error field correction coils.

A definitive size scaling experiment is ongoing between JET, DIII-D, and Alcator C-Mod[75,77] that spans approximately a factor 4 in linear size. In this experiment the same equilibria in terms of nondimensional parameters (plasma shape, q_{95}, etc.) are used in the three tokamaks. Also, the applied error field spectra are chosen to be very similar to that of the JET EFCCs, by exploiting the flexibility of the DIII-D and Alcator C-Mod error field coil systems. For equilibria corresponding to $I_p = 0.88$ MA and $B_T = 0.98$ T in JET (scaled to the other tokamaks with $B_T a^{5/4}$ constant), the locked mode thresholds as a function of density have been compared. In terms of scale invariance considerations, equilibria with the same nondimensional parameters will have a constant value of $n_e a^2$, and in Fig. 20 the locked mode density threshold is shown with the plasma densities in JET scaled to the equivalent Alcator C-mod value. From Fig. 20 it can be seen that the dimensionally scaled error field locked mode thresholds in JET and Alcator C-Mod are in good agreement, whereas it has been found that the DIII-D threshold is somewhat higher.[75]

III.B. Improvement in Operating Domain

As with several other tokamaks (e.g., Refs. 78 and 79), JET has demonstrated an extended operational domain in discharges with error correction. Figure 21 shows how with correction of the measured intrinsic error, a 35% lower density can be reached before a locked mode forms.

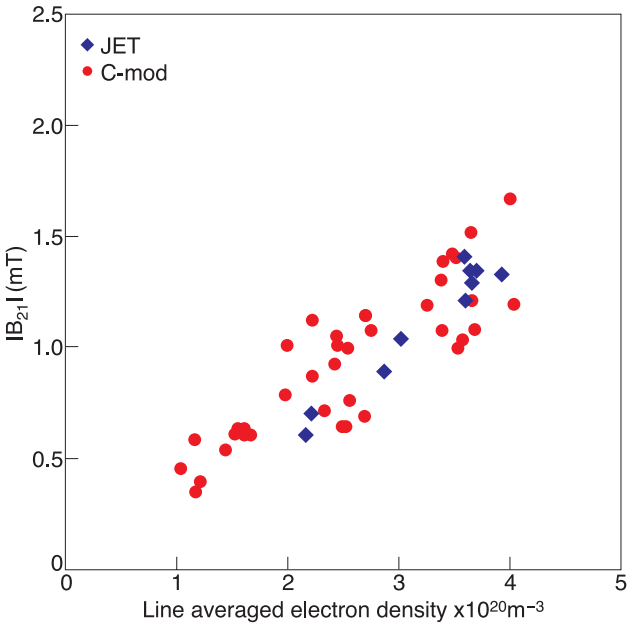

Fig. 20. Locked mode thresholds compared between dimensionally equivalent discharges in JET and Alcator C-Mod. In this plot the underlying values of density and error field are scaled (as discussed in the text) to their equivalent values in Alcator C-mod. The error field $B_{2,1}$ is the sum of the applied and measured/deduced error field (except for JET, where the intrinsic error is low enough to be ignored in this case).[77]

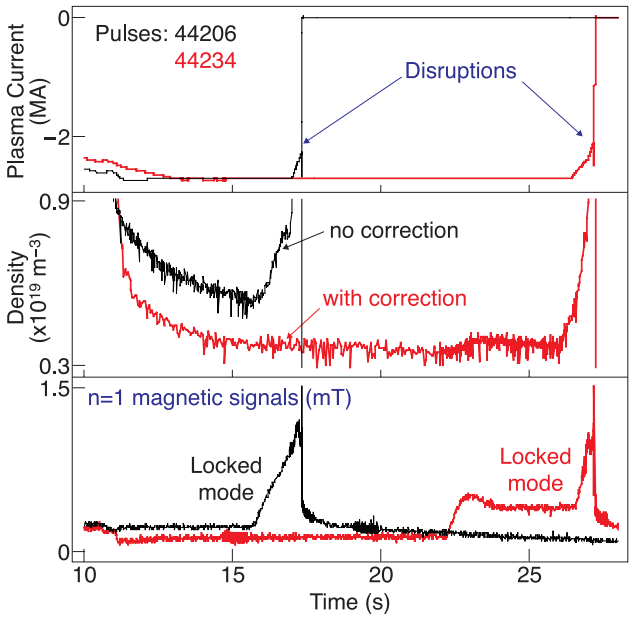

Fig. 21. With correction of the intrinsic error, a 35% lower density can be achieved before an error field locked mode forms. This result is consistently reproducible, as discussed in Ref. 29.

Once an error field locked mode has formed there is a hysteresis, which means that it tends to persist, and even if a prompt disruption does not occur, one often occurs when the plasma current is ramped down. Experiments in JET (Ref. 29) showed that by correcting the intrinsic error field, a preexisting locked mode could be made to rotate and decay (a process termed *spin-up*). In a series of 35 pulses, 10 had the intrinsic error field corrected following locked mode formation, and in this case only 20% disrupted, whereas in the uncorrected pulses 84% disrupted (mainly as the plasma current was ramped down to terminate the pulse). These results show the value of error field correction. However, the intrinsic error fields on JET are relatively low and routine error field correction is not employed, unlike some other tokamaks, e.g., DIII-D (Ref. 78).

III.C. Physics of Error Field Locking

The basic physics principles underlying error field locking are well established[26]; however, certain issues connected with the underlying causes of mode rotation and mode coupling issues, among others, remain to be resolved.

Studies on JET (Ref. 80) show that an improved description of error field mode locking data is obtained by including a theoretically predicted form of the plasma rotation into the scaling for the threshold error field to form an $m = 2$, $n = 1$ locked mode. These experiments used plasmas with low levels of neutral beam to drive modest levels of rotation and obtain rotation measurements from charge exchange recombination spectroscopy. It is found that the variation of the locked mode threshold is well described by the scaling relation $B_{pen}/B_T \propto n^{0.58} B_T^{-1.27} \omega_0^{1/2}$ (where ω_0 is the preerror field fluid rotation frequency at $q = 2$). Further, a good match to theory has been achieved, with locked mode formation being precipitated after the electromagnetic torque has slowed the plasma to half its original frequency. The results have also shed light on the important physics of plasma rotation braking from applied helical "error fields." A viscous drag model with the torque applied solely at the island ($q = 2$) surface would predict a uniform reduction of the rotation within $q = 2$, but the observations[80,81] seem to contradict this and indicate an approximately self-similar reduction of plasma rotation within $q = 2$ (Fig. 22).

A new model associated with a toroidal viscous drag originating from nonaxisymmetric fields, in particular due to the nonresonant $m = 0$, $n = 1$ mode, seems to qualitatively match these observations[80]; however, a more complete treatment including mode coupling due to toroidal and shaping effects[82] is needed to fully understand the fluid rotation behavior.

III.D. Effect of β on Error Field–Driven Locked Mode

Initially, as β is increased with neutral beam injection (NBI) heating, the error threshold rises; as discussed

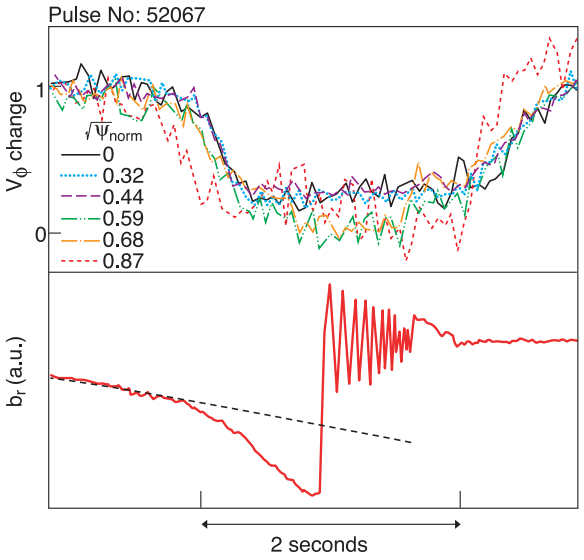

Fig. 22. Change of toroidal velocity (top, normalized to its value just before the error field is applied) for a range of radii (described in terms of normalized poloidal flux) within $q = 2$. Measured radial magnetic field (bottom). The error field locked mode is induced when this signal departs from linear ramp (indicated by the broken line) expected from a direct response to linearly ramped error field. As the error field is turned off, a slowly rotating island occurs, which slowly decays and increases in frequency. The plasma toroidal velocity then approximately returns to its initial value.

in the previous subsection, at low β the error field threshold's rise with the beam-induced rotation is best fitted as $\sqrt{\omega_0}$. In contrast, equivalent plasmas in which ICRF heating alone was used in JET to increase β showed only a small increase in the error field threshold,[29] presumably due to the low induced rotation. At higher β, as the ideal stability limit is approached, the error field threshold decreases with rising β, as first reported in Ref. 83 for the DIII-D tokamak. It is now understood that as the ideal β limit is approached in low-collisionality ELMy H-mode plasmas, $m = 2, n = 1$ NTMs are likely to be destabilized just below the ideal limit.[65] As discussed in Sec. II.E, studies on JET (Ref. 67) indicate a reduction of error field threshold near the 2/1 NTM β limit (Fig. 12), although the exact mechanism (through error field drives or changes in NTM stability in response to plasma braking) cannot be resolved.

In advanced scenarios in which $m = 2, n = 1$, NTMs may be precluded by the q profile (i.e., $q > 2$ everywhere), then at high β RWMs may be destabilized. These RWMs are ideal instabilities whose growth rate is slowed to the wall time constant and which can be stabilized by sufficiently high plasma rotation speeds. As RWM instability is approached, error field locked modes also become increasingly easy to form, as discussed in the next section.

IV. RESISTIVE WALL MODE STUDIES

Resistive wall modes occur when β exceeds the no-wall β limit (the limit predicted with a vacuum surrounding the plasma) but lies below the with-wall β limit (the limit that would result if the wall surrounding the plasma were a perfect conductor).

JET has studied advanced scenarios with an axial safety factor $q_0 \sim 2$ for a number of years. In these cases the high β achieved may destabilize kink modes with a substantial external component, as discussed in Ref. 84. These kink modes generally form at an observed rotation speed of several kHz, so the wall and other conducting structures surrounding the plasma act as perfect conductors, shielding flux penetration from the mode. In fact, in such cases the kink modes tend to be destabilized by the strong pressure gradients occurring at internal transport barriers,[84,85] and the presence of a wall, as opposed to a surrounding vacuum, increases the stability margin in β by about 10 to 15%. So the band in which resistive wall modes might occur, between the no-wall and with-wall β limits, is relatively narrow in this type of discharge (see Sec. V.A of Ref. 86).

This relatively narrow band between the no-wall and with-wall β limits combined with the tendency of discharges to rapidly traverse the band means that natural RWMs have not been conclusively observed in JET, though there are a few pulses in which slowly rotating modes ($\omega\tau_w \sim 1$, where ω is mode rotation and τ_w is wall time constant) have been observed that might be RWMs, as discussed in Ref. 87.

Though intrinsically unstable RWMs have not been conclusively observed in JET, substantial progress has been made by using MHD spectroscopy–type techniques to probe stable RWMs and by magnetically braking the plasma, thereby destabilizing RWMs; these RWM studies in JET are discussed in the next two subsections.

IV.A. MHD Spectroscopy of RWMs

The stability of stable MHD modes may be probed by applying suitable external magnetic perturbations and measuring the response of the plasma. In particular for RWMs, as the no-wall β limit is exceeded, strong amplification of applied resonant fields occurs[88]—this is termed resonant field amplification (RFA). Since the RFA increases as the RWM damping decreases, RFA measurements represent a means to determine plasma damping. Also, theoretical damping models, implemented in MHD codes, may be validated by comparison with RFA measurements.

Both the internal saddle coils (Fig. 17a) and EFCCs (Fig. 17b) have been used to measure RFA. Figure 23a shows how the RFA increases as β rises above the empirical no-wall limit, which is determined by calculation (and empirically; see Sec. III.B) to be $3.4l_i$ [where $l_i = 2V\langle B_p^2\rangle/(\mu_0^2 I_p^2 R)$, with V = plasma volume being the

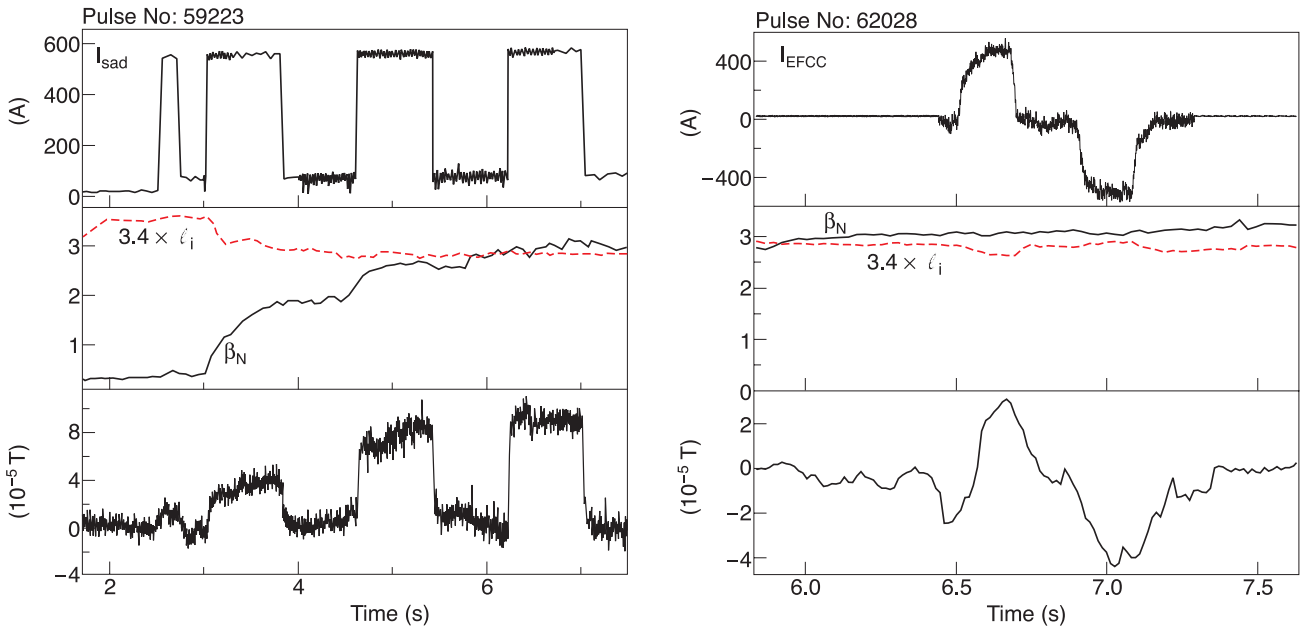

(a) (b)

Fig. 23. (a) Currents are applied in one pair of the internal saddle coils as the no-wall β limit is approached and exceeded, so the measured $n = 1$ outboard midplane radial field increases (the position from which this measurement is taken is such that without a plasma, it has no direct pickup of the applied field). (b) RFA from EFCCs.

internal inductance] for these discharges, which have a central $q_0 \sim 1.5$. Similarly, Fig. 23b shows RFA occurring from fields applied using the EFCCs.

As mentioned in the introduction, the RFA may be compared against various theoretical models of RWM damping, and in the case of JET this has been done using the MARS-F MHD stability code.[89] In MARS-F an RWM damping model based on ion Landau damping[90] has been used extensively. In this model the force that damps the (m, n) Fourier component of the perturbed toroidal motion of the plasma is represented as a parallel viscosity term, $F_{damp} = -\kappa_{\|}|k_{\|}v_{th,i}|\rho v_{\|}$, where $k_{\|} = (m/q - n)/R$ is the parallel wave number, $v_{th,i}$ is the ion thermal velocity, ρ is the mass density, $v_{\|}$ is the perturbed parallel velocity of the plasma, and $\kappa_{\|}$ is a constant whose value may be empirically determined by fitting to experimental results. Also, a more accurate "kinetic" model[91] based on drift-kinetic theory has been implemented in the MARS-F stability code to predict the forces acting on the displacements perpendicular to the magnetic field; it is important to note that this kinetic model has no free-fitting parameters. The RFA defined as $|B_r - B_r(vac)|/|B_r(vac)|$, where the radial field (B_r) is measured on the outboard midplane just outside the vacuum vessel, is shown in Fig. 24 for the case of the internal saddle coils.[92] The comparisons with MARS-F calculations show that both strong parallel damping, $\kappa_{\|} \sim 1$, and the kinetic model give good agreement with the data. The kinetic model is

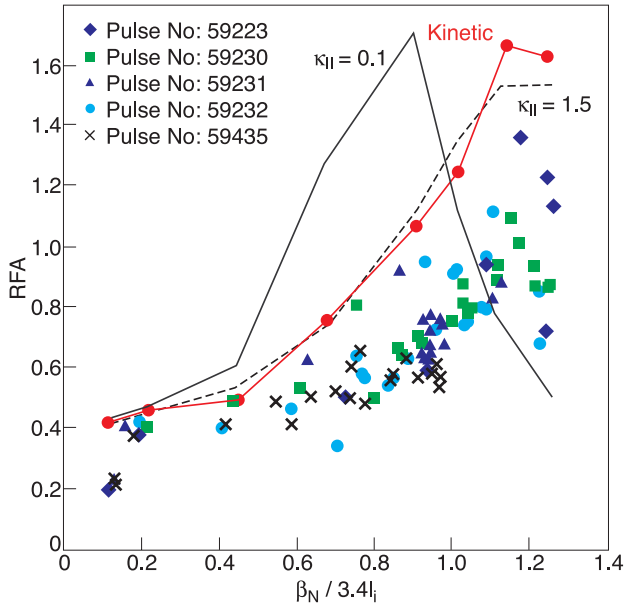

Fig. 24. RFA measured with midplane B_r coils arising from fields applied using the internal error field coils. β_N is normalized with respect to the approximate no-wall limit, $3.4l_i$. Each symbol type represents a different pulse. The curves show the predictions of various damping models in the MARS-F code—both the kinetic model and strong parallel damping is in reasonable agreement.[92]

expected to lead to strong damping because even when the flow is strongly subsonic, there will be regions close to resonant surfaces where the parallel phase velocity in the plasma frame is large enough to resonate with thermal particles giving rise to strong local damping. The RFA has also been measured using the external EFCCs on JET and equivalently good agreement between the data and the kinetic damping model is found.

Joint experiments on RFA with the DIII-D tokamak have also been conducted[93] using plasmas closely matched in terms of shape, pressure, and q profiles. There are differences in the geometry of the coil systems used to apply the resonant fields and also in the geometry of the detector coil system. These geometry differences can be compensated for, and the simplest approach is to assume cylindrical geometry and that the main harmonic involved is $m = 2$. When this simple approach is applied, the RFA observed in JET and DIII-D are in reasonable agreement[94] (Fig. 25); here, the degree to which the no-wall β limit is exceeded is measured using $C_\beta = [\beta - \beta_N(no\text{-}wall)]/[\beta_N(wall) - \beta_N(no\text{-}wall)]$. Figure 25 also shows a comparison of the RFA with various MARS-F calculations. Again the kinetic model and strong sound wave damping ($\kappa_\parallel = 1.5$) show reasonable agreement with experiment.

It is found that the plasma rotation in the vicinity of $q = 2$, when normalized by the Alfvén time ($\Omega_{q=2}\tau_A$), is comparable in JET and DIII-D (in the core they differ). So the equivalence of the RFA in JET and DIII-D, which itself depends on the plasma damping arising from rotation, is consistent with that damping being a function of rotation in the vicinity of $q = 2$ normalized by the Alfvén time.

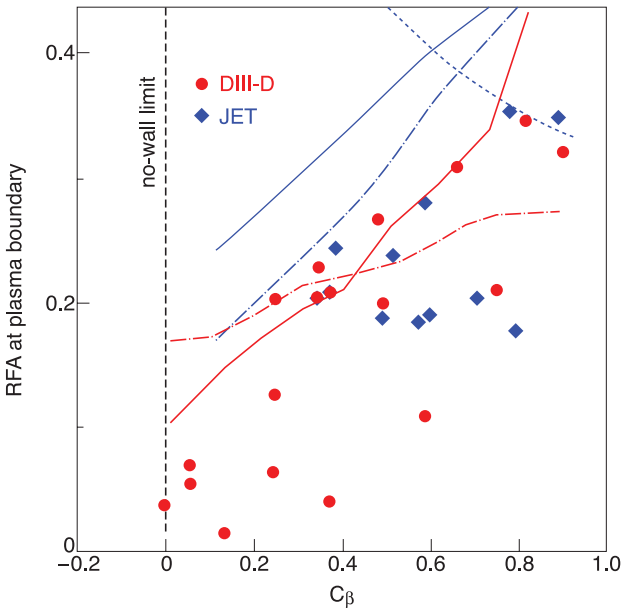

Fig. 25. RFA versus $C_\beta = [\beta_N - \beta_N(no\text{-}wall)]/[\beta_N(wall) - \beta_N(no\text{-}wall)]$. Geometric differences between the JET and DIII-D coil systems are accounted for, as explained in the text. Here, the dashed-dotted lines are calculations using the kinetic damping model in the MARS-F MHD stability code.[87] The solid lines are the sound wave model with strong damping ($\kappa_\parallel = 1.5$) and the dotted line is weak damping ($\kappa_\parallel = 0.1$). The red (or light) lines are based on a DIII-D equilibrium and the blue (or dark) lines on a JET equilibrium (for clarity, the weak kinetic damping model is not shown for DIII-D—the agreement is equally as bad as for the JET case). From Ref. 94.

IV.B. Measurement of RWM Critical Velocity

The occurrence of a critical flow velocity below which the RWM becomes unstable can also be compared with modeling. In JET the flow velocities due to NBI are fairly high (~1% of $V_{Alfvén}$ at $q = 2$), whereas the predicted critical velocity for RWMs is ~0.5% of $V_{Alfvén}$. An ~30% reduction of plasma velocity was achieved by substituting ~4 MW of NBI with ICRH. Further reduction of the velocity, however, required magnetic braking using the error field coils. Employing this technique, an intrinsically unstable mode is found to grow below a critical velocity, leading to severe confinement degradation, and at lower q_{95} (~3) to disruptions (Fig. 26). It should be

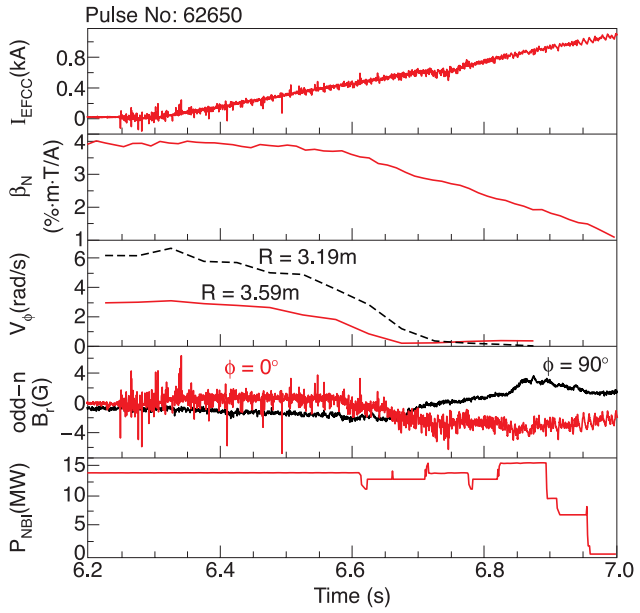

Fig. 26. $q_{95} = 3.2$ pulse in which application of an applied field with the EFCCs at high β_N leads to mode-locking, as seen on the plasma velocity (V_ϕ) and the quadrature pair of odd-n B_r signals (with direct vacuum pickup from the EFCCs eliminated). As the RWM develops from $t = 6.65$ s the confinement is severely degraded, as evidenced by the decline in β_N. Shortly beyond the time shown a disruption occurs. From Ref. 92.

noted that in this technique the applied error field may not only be braking the plasma but also contributing to driving the RWM (Ref. 95), meaning the observed flow velocities at which the RWM is destabilized should be regarded as an upper bound.

There seems to be a threshold in β_N below which the magnetic braking is not effective (Fig. 27), which is interpreted as β_N being below the no-wall β limit; this value of $\beta_N/l_i \sim 3.3$ is consistent with the no-wall β limit (discussed in the previous subsection). It should be noted that there is no 2/1 NTM observed in these cases, so the observed braking is not due to a large NTM locking to the wall.

The critical rotation velocity (Ω_{crit}) for RWM formation has also been compared between JET and DIII-D (Ref. 93). As for the RFA comparison (discussed above), matched plasmas between the two devices are used, and in agreement with the RFA studies it is found that the critical rotation velocity at $q = 2$ normalized by the Alfvén time $[\Omega_{crit}(q = 2)\tau_A]$ have approximately the same value in JET and DIII-D. In contrast, the axial values of $\Omega_{crit}(q = 2)\tau_A$ differ strongly between JET and DIII-D. So again there is an indication that velocity in the vicinity of $q = 2$, normalized by τ_A, is the factor controlling RWM damping, though the role played by the applied error fields in driving the RWM (Ref. 95) may influence the interpretation of this result.

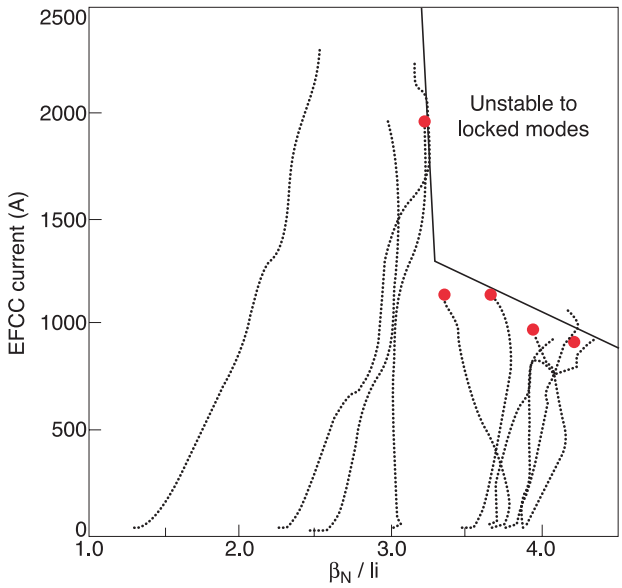

Fig. 27. Trajectories of discharges in which EFCC currents are applied to brake the plasma. The closed circles represent the points at which sufficient braking occurs for an RWM to be destabilized. RWMs are not observed below $\beta_N/l_i \sim 3.3$, which is interpreted as the no-wall limit and is consistent with calculations discussed in the previous subsection, which gave $\beta_N/l_i \sim 3.4$. From Ref. 92.

V. CONCLUSIONS

We have seen that from strong beginnings that established many of the fundamentals of tokamak stability physics experimentally, JET has continued to address the vital questions of stability physics as the understanding of the underlying physics and the key points of concern has evolved.

On NTM physics, many of the basic properties have been confirmed, with JET providing key "nearest ITER" data (in terms of ρ^*) for international databases and extrapolations. The seeding process and the role of small island size stabilization terms have been explored in detail, with various models being tested and good candidate mechanisms being elucidated. JET has identified a range of NTM triggering mechanisms, with different processes applying in different parameter regimes and sometimes more than one process active in a given regime. These observations are helping to identify the specific physics processes involved and the issues for ITER. So far, the main concern for the ITER baseline scenario comes from sawtooth-triggered 3/2 and 2/1 NTMs. Other mechanisms of NTM triggering for the 3/2 and 2/1 NTMs have so far been confined to higher-β_N regimes, at least at JET. For hybrid scenario, preliminary JET data, now being combined with cross-machine databases, show no indications of an adverse ρ^* scaling taking the threshold to low β_N as low ρ^* values are accessed on JET.

Focusing on the key issue of sawtooth-triggered NTMs for the baseline scenario, new techniques that may prove essential for ITER, such as the control of fast-particle-stabilized sawteeth, have been pioneered at JET. There are also encouraging developments in the understanding of the sawteeth, with a quantitatively predictive theory now lying within our grasp. It seems likely that the required destabilization of fast-particle-stabilized sawteeth is achievable and could be developed as a tool prior to ITER operation. As a result of the work on JET and elsewhere, the likely behavior and requirements of NTMs are becoming clearer for ITER. NTM and sawtooth physics remains a challenging area, but one in which progress is beginning to pay off in terms of theoretical and experimental tools to predict and control behavior.

MHD studies of error field–induced locked modes and resistive wall modes have made important contributions to understanding in these areas. The error field threshold scalings derived from systematic studies in JET predict a threshold for the ITER FDR reference parameters of $B_{2,1}/B_T$ of 1.25×10^{-4}, a value that is well within the capabilities of the proposed ITER error correction coils, a conclusion that is supported by ongoing cross-machine identity experiments.[75] Error field studies in JET have also helped clarify the role of nonresonant harmonics in contributing to the plasma braking that allows locked mode formation.

At higher β error field physics becomes linked with NTM and/or RWM stability thresholds. In particular for

RWMs, the amplification of applied error fields (RFA) is an excellent diagnostic of the degree of rotational damping of the mode. Also, error fields can be used to magnetically brake the plasma, allowing RWM instability, though the error field may also directly drive the RWM in this case.[95] In both of these areas of RWM study, joint experiments with the DIII-D tokamak have indicated that the plasma rotation near the edge (in the $q = 2$ vicinity) normalized to the Alfvén velocity is the controlling parameter for RWM damping. Further direct inference from these experimental RWM results and the benchmarking of the MARS-F code have both quantitatively and qualitatively improved understanding of RWM stability in ITER.

These studies show that through its size and the parameters that JET can access, it is continuing, and will continue, to answer the leading questions on plasma stability. The coming enhancements on JET—new ITER-like ICRF antenna and more NBI power, together with an ITER-like wall—will provide further key capabilities, improving control over fast-particle populations and operating closer to ITER's ρ^*, and with reduced momentum injection, allowing JET to access more ITER-relevant plasma regimes for the study of stability physics.

ACKNOWLEDGMENTS

The authors thank J. P. Graves for his useful contribution to the text, as well as acknowledging the valuable contributions and discussions with the many colleagues listed in the references that have provided the basis for this paper. This work was conducted under the European Fusion Development Agreement and jointly supported by the United Kingdom Engineering and Physical Sciences Research Council and by the European Communities under the contract of association between EURATOM and UKAEA. The views and opinions expressed herein do not necessarily reflect those of the European Commission.

REFERENCES

1. P. H. REBUT et al., "The Joint European Torus: Installation, First Results and Prospects," *Nucl. Fusion*, **25**, 1011 (1985).

2. J. A. WESSON et al., "Density Limit Disruptions in JET," *Proc. 12th European Conf. Controlled Fusion and Plasma Physics*, Vol. I, p. 147 (1985).

3. A. GIBSON, "Radiation Limits to Tokamak Operation," *Nucl. Fusion*, **16**, 546 (1976).

4. J. A. WESSON et al., "Disruptions in JET," *Nucl. Fusion*, **29**, 641 (1989).

5. D. J. WARD et al., "Impurity Influx Modes of Fast Tokamak Disruptions," *Nucl. Fusion*, **32**, 1117 (1992).

6. D. J. CAMPBELL et al., "Analysis of Sawtooth Instabilities in JET," *Proc. 12th European Conf. Controlled Fusion and Plasma Physics*, Vol. I, p. 130 (1985).

7. J. A. WESSON, "Sawtooth Oscillations," *Plasma Phys. Controll. Fusion*, **28**, 243 (1986).

8. J. A. WESSON et al., "Sawtooth Reconnection," *Nucl. Fusion*, **30**, 2545 (1990).

9. D. J. C. CAMPBELL et al., "Stabilization of Sawteeth with Additional Heating in the JET Tokamak," *Phys. Rev. Lett.*, **60**, 2148 (1988).

10. F. PORCELLI, "Fast Particle Stabilisation," *Plasma Phys. Controll. Fusion*, **33**, 1601 (1991).

11. J. PAMELA et al., "Overview of Results and Possibilities for Fast Particle Research on JET," *Nucl. Fusion*, **42**, 1014 (2002).

12. V. P. BHATNAGAR et al., "Local Magnetic Shear Control in a Tokamak via Fast Wave Minority Ion Current Drive: Theory and Experiments in JET," *Nucl. Fusion*, **34**, 1579 (1994).

13. O. SAUTER et al., "Control of Neoclassical Tearing Modes by Sawtooth Control," *Phys. Rev. Lett.*, **88**, 105001 (2002).

14. L. G. ERIKSSON et al., "Destabilization of Fast-Ion-Induced Long Sawteeth by Localized Current Drive in the JET Tokamak," *Phys. Rev. Lett.*, **92**, 235004 (2004).

15. T. C. HENDER et al., "MHD Stability with Strongly Reversed Magnetic Shear in JET," *Plasma Phys. Controll. Fusion*, **44**, 1143 (2002).

16. R. J. BUTTERY et al., "Neoclassical Tearing Modes," *Plasma Phys. Controll. Fusion*, **42**, B61 (2000).

17. M. R. WADE et al., "Development, Physics Basis and Performance Projections for Hybrid Scenario Operation in ITER on DIII-D," *Nucl. Fusion*, **45**, 407 (2005).

18. O. GRUBER et al., "ITER Operation Beyond Its Baseline Scenario," *Plasma Phys. Controll. Fusion*, **47**, B135 (2005).

19. Y. KAMADA et al., "Extended JT-60U Plasma Regimes for High Integrated Performance," *Nucl. Fusion*, **41**, 1311 (2001).

20. R. J. BUTTERY et al., "Cross-Machine NTM Physics Studies and Implications for ITER," *Proc. 20th Int. IAEA Conf. Fusion Energy*, Vilamoura, Portugal, EX-7/1 (2004).

21. J. A. SNIPES et al., "Large Amplitude Quasi-Stationary MHD Modes in JET," *Nucl. Fusion*, **28**, 1085 (1988).

22. J. A. SNIPES et al., "Plasma Stored Energy and Momentum Losses During Large MHD Activity in JET," *Nucl. Fusion*, **30**, 205 (1990).

23. T. C. HENDER et al., "Effects of a Resistive Wall on Magnetohydrodynamic Instabilities," *Nucl. Fusion*, **29**, 1279 (1989).

24. M. F. F. NAVE et al., "Mode Locking in Tokamaks," *Proc. 13th European Conf. Controlled Fusion and Plasma Physics*, Vol. III, p. 1103 (1987).

25. T. C. HENDER et al., "Disruption Control in the Tokamak," *Proc. 12th Int. Conf. Plasma Physics and Controlled Fusion*, Nice, France, IAEA, Vienna, Austria (1988).

26. R. FITZPATRICK and T. C. HENDER, "Effect of a Static External Magnetic Perturbation on Resistive Mode Stability in Tokamaks," *Phys. Plasmas*, **1**, 3337 (1994).

27. A. W. MORRIS et al., "Driven Magnetic Reconnection in the COMPASS-C Tokamak," *Phys. Fluids*, **4**, 413 (1992).

28. G. M. FISHPOOL and P. S. HAYNES, "Field Error Instabilities in JET," *Nucl. Fusion*, **34**, 109 (1994).

29. R. J. BUTTERY et al., "Error Field Experiments in JET," *Nucl. Fusion*, **40**, 807 (2000).

30. A. M. GAROFALO et al., "Sustained Rotational Stabilization of DIII-D Plasmas Above the No-Wall Beta Limit," *Phys. Plasmas*, **9**, 1997 (2002).

31. R. CARRERA et al., "Island Bootstrap Current Modification of the Nonlinear Dynamics of the Tearing Mode," *Phys. Fluids*, **29**, 899 (1986).

32. O. SAUTER et al., "Beta Limits in Long-Pulse Tokamak Discharges," *Phys. Plasmas*, **4**, 1654 (1997).

33. O. SAUTER et al., "Neoclassical Conductivity and Bootstrap Current Formulas for General Axisymmetric Equilibria and Arbitrary Collisionality Regime," *Phys. Plasmas*, **6**, 2834 (1999); see also O. SAUTER et al., *Phys. Plasmas*, **9**, 5140 (2002).

34. H. LUTJENS et al., "Curvature Effects on the Dynamics of Tearing Modes in Tokamaks," *Phys. Plasmas*, **8**, 4267 (2001).

35. R. B. WHITE et al., "Saturation of the Tearing Mode," *Phys. Fluids*, **20**, 800 (1977).

36. R. FITZPATRICK et al., "Helical Temperature Perturbations Associated with Tearing Modes in Tokamak Plasmas," *Phys. Plasmas*, **2**, 825 (1995).

37. H. R. WILSON et al., "Threshold for Neoclassical Magnetic Islands in a Low Collision Frequency Tokamak," *Phys. Plasmas*, **3**, 248 (1996).

38. E. POLI et al., "Reduction of the Ion Drive and ρ_θ^* Scaling of the Neoclassical Tearing Mode," *Phys. Rev. Lett*., **88**, 075001 (2002).

39. H. R. WILSON et al., "The Collisionality Dependence of Tokamak β-Limits," *Plasma Phys. Controll. Fusion*, **38**, A149 (1996).

40. R. J. LA HAYE et al. "Dimensionless Scaling of the Critical Beta for Onset of a Neoclassical Tearing Mode," *Phys. Plasmas*, **7**, 3349 (2000).

41. H. ZOHM et al., "Neoclassical Tearing Modes and Their Stabilization by Electron Cyclotron Current Drive in ASDEX Upgrade," *Phys. Plasmas*, **8**, 2009 (2001).

42. Z. CHANG and J. D. CALLEN, *Phys. Fluids B*, **4**, 1182 (1992).

43. Z. CHANG et al., "Observation of Nonlinear Neoclassical Pressure-Gradient–Driven Tearing Modes in TFTR," *Phys. Rev. Lett*., **74**, 4663 (1995).

44. G. T. A. HUYSMANS et al., "Observation of Neoclassical Tearing Modes in JET," *Nucl. Fusion*, **39**, 1965 (1999).

45. O. SAUTER et al. "Marginal β-Limit for Neoclassical Tearing Modes in JET H-Mode Discharges," *Plasma Phys. Controll. Fusion*, **44**, 1999 (2002).

46. R. J. BUTTERY et al., "Onset of Neoclassical Tearing Modes on JET," *Nucl. Fusion*, **43**, 69 (2003).

47. T. C. HENDER et al., "Comparison of $m = 2$, $n = 1$ Neo-Classical Tearing Mode Limits in JET and DIII-D," *Nucl. Fusion*, **44**, 788 (2004).

48. R. J. BUTTERY et al., "On the Form of NTM Onset Scalings," *Nucl. Fusion*, **44**, 678 (2004).

49. F. PORCELLI et al., "Predicting the Behaviour of Magnetic Reconnection Processes in Fusion Burning Plasma Experiments," *Nucl. Fusion*, **44**, 362 (2004).

50. A. MÜCK et al., "NTM Control via Sawtooth Tailoring in ASDEX Upgrade," *Proc. 30th European Conf. Plasma Physics and Controlled Fusion*, St. Petersburg, Russia, ECA 27A, P-1.131 (2003).

51. F. PORCELLI et al., "Model for the Sawtooth Period and Amplitude," *Plasma Phys. Controll. Fusion*, **38**, 2163 (1996).

52. L.-G. ERIKSSON et al., "On Ion Cyclotron Current Drive for Sawtooth Control," *Nucl. Fusion*, **46**, S951 (2006).

53. M.-L. MAYORAL et al., "Studies of Burning Plasma Physics in the Joint European Torus," *Phys. Plasmas*, **11**, 2607 (2004).

54. G. J. KRAMER et al., "Fast Particle Experiments in JT-60U," *Nucl. Fusion*, **40**, 1383 (2000).

55. J. P. GRAVES, "Influence of Asymmetric Energetic Ion Distributions on Sawtooth Stabilization," *Phys. Rev. Lett*., **92**, 185003 (2004).

56. M. F. F. NAVE et al., "Exploring a Small Sawtooth Regime in Joint European Torus Plasmas with Counterinjected Neutral Beams," *Phys. Plasmas*, **13**, 014503 (2006).

57. J. P GRAVES et al., "The Effects of Sheared Toroidal Plasma Rotation on the Internal Kink Mode in the Banana Regime," *Plasma Phys. Controll. Fusion*, **42**, 1049 (2000).

58. J. P. GRAVES et al., "Sawtooth Control in Fusion Plasmas," *Plasma Phys. Controll. Fusion*, **47**, B121 (2005).

59. I. T. CHAPMAN et al., "Modeling the Effect of Toroidal Plasma Rotation on Drift-Magnetohydrodynamic Modes in Tokamaks," *Phys. Plasmas*, **13**, 062511 (2006).

60. C. C. HEGNA et al., "Dynamics of Seed Magnetic Island Formation Due to Geometrically Coupled Perturbations," *Phys. Plasmas*, **6**, 130 (1999).

61. M. F. F. NAVE et al., "Triggering of Neo-Classical Tearing Modes by Mode Coupling," *Nucl. Fusion*, **43**, 179 (2003).

62. C. C. HEGNA, "Seeding Neoclassical Tearing Modes by Transient Transport Events," *Bull. Am. Phys. Soc*., QP1.115 (2003).

63. P. BELO et al., "Observation and Implication of MHD Modes for the Hybrid Scenario in JET," *Proc. 31st European Conf. Plasma Physics and Controlled Fusion*, London, United Kingdom, ECA 28G, P-1.1.70 (2004).

64. E. JOFFRIN et al., "The 'Hybrid' Scenario in JET: Towards Its Validation for ITER," *Nucl. Fusion*, **45**, 626 (2005).

65. D. P. BRENNAN et al., "Tearing Mode Stability Studies Near Ideal Stability Boundaries in DIII-D," *Phys. Plasmas*, **9**, 2998 (2002).

66. D. P. BRENNAN et al., "A Mechanism for Tearing Onset Near Ideal Stability Boundaries," *Phys. Plasmas*, **10**, 1643 (2003).

67. R. J. BUTTERY et al., "Interplay of Error Field and Neoclassical Tearing Mode Drives and Rotation for the 2-1 Mode in JET and DIII-D," *Proc. 32nd European Conf. Plasma Physics and Controlled Fusion*, Terragona, Spain, ECA 29c, P5-060 (2005).

68. A. GÜDE et al., "Seed Island of Neoclassical Tearing Modes at ASDEX Upgrade," *Nucl. Fusion*, **39**, 127 (1999).

69. R. J. LA HAYE et al., "Cross-Machine Benchmarking for ITER of Neoclassical Tearing Mode Stabilization by Electron Cyclotron Current Drive," *Nucl. Fusion*, **46**, 451 (2006).

70. T. C. HENDER et al., "Trace-Tritium Measurement of Magnetic Island Effect on Particle Confinement," *Proc. 31st European Conf. Plasma Physics and Controlled Fusion*, ECA 28G, P-1.163 (2004).

71. S. GUNTER et al., "The Frequently Interrupted Regime of Neoclassical Tearing Modes (FIR-NTMs): Required Plasma Parameters and Possibilities for Its Active Control," *Nucl. Fusion*, **44**, 524 (2004).

72. S. GÜNTER et al., "High Confinement Regime in the Presence of (3,2) Neoclassical Tearing Modes," *Proc. 28th European Conf. Plasma Physics and Controlled Fusion*, Funchal, Portugal (2001).

73. T. C. HENDER et al., "Effect of Resonant Magnetic Perturbations on COMPASS-C Tokamak Discharges," *Nucl. Fusion*, **32**, 2091 (1992).

74. ITER PHYSICS BASIS, *Nucl. Fusion*, **39**, 2137 (1999).

75. S. M. WOLFE et al., "Nonaxisymmetric Field Effects on Alcator C-Mod," *Phys. Plasmas*, **12**, 056110 (2005).

76. J. W. CONNOR and J. B. TAYLOR, "Scaling Laws for Plasma Confinement," *Nucl. Fusion*, **19**, 1047 (1977).

77. D. F. HOWELL et al., "Machine Size Scaling of Error Field Induced Locked Mode-Thresholds," *Proc. 46th Annual Mtg. Division of*

Plasma Physics, Savannah, Georgia, paper CP1.020, American Physical Society (2004).

78. J. T. SCOVILLE and R. J. LA HAYE, "Multi-Mode Error Field Correction on the DIII-D Tokamak," *Nucl. Fusion*, **43**, 250 (2003).

79. D. F. HOWELL et al., "Locked Mode Thresholds on the MAST Spherical Tokamak," *Nucl Fusion*, **47**, 1336 (2007).

80. E. LAZZARO et al., "Error Field Locked Mode Thresholds in Rotating Plasmas, Anomalous Braking and Spin-Up," *Phys. Plasmas*, **9**, 3906 (2002).

81. T. C. HENDER et al., "Sawtooth, Neo-Classical Tearing Mode and Error Field Studies in JET," *Proc. 19th Int. Conf. Fusion Energy*, Lyon, France, EX/S1-2, IAEA, Vienna (2002) (CD-ROM; available on the Internet at http://www.iaea.org/programmes/ripc/physics/fec2002/html/fec2002.htm).

82. E. LAZZARO and P. ZANCA, "Effects of a Nonresonant $m = 0$, $n = 1$ Perturbation Driven by Coupling to the $m = 2$, $n = 1$ Mode in an Elongated Tokamak," *Phys. Plasmas*, **10**, 2399 (2003).

83. R. J. LA HAYE et al., "Nonlinear Instability to Low $m, n = 1$ Error Fields in DIII-D as a Function of Plasma Fluid Rotation and Beta," *Nucl. Fusion*, **32**, 2119 (1992).

84. G. T. A. HUYSMANS et al., "MHD Stability of Optimized Shear Discharges in JET," *Nucl. Fusion*, **39**, 1489 (1999).

85. T. C. HENDER et al., "Variation of MHD Stability in JET Optimized Shear Discharges," *Proc. 26th European Conf. Controlled Fusion and Plasma Physics*, **23J**, 89 (1999).

86. C. GORMENZANO et al., "Advanced Tokamak Scenario Development at JET," *Fusion Sci. Technol.*, **53**, 958 (2008).

87. M. P. GRYAZNEVICH et al., "Resistive Wall Mode Studies on JET," *Bull. Am. Phys. Soc.*, **48**, RP1.036 (2003).

88. A. H. BOOZER, "Error Field Amplification and Rotation Damping in Tokamak Plasmas," *Phys. Rev. Lett.*, **86**, 5059 (2001).

89. Y. Q. LIU et al., "Feedback Stabilization of Nonazisymmetric Resistive Wall Modes in Tokamaks. 1. Electromagnetic Modes," *Phys. Plasmas*, **7**, 3681 (2000).

90. A. BONDESON and D. WARD, "Stabilization of External Modes in Tokamaks by Resistive Walls and Plasma Rotation," *Phys. Rev. Lett.*, **72**, 2709 (1994).

91. A. BONDESON and M. S. CHU, "Inertia and Ion Landau Damping of Low-Frequency Magnetohydrodynamical Modes in Tokamaks," *Phys. Plasmas*, **3**, 3013 (1996).

92. T. C. HENDER et al., "Resistive Wall Mode Studies in JET," *Proc. 20th Int. Conf. Fusion Energy*, Vilamoura, Portugal, EX/P2-22, IAEA, Vienna, Austria (2004) (CD-ROM); available on the Internet at http://www.naweb.iaea.org/napc/physics/fec/fec2004/index.html.

93. H. REIMERDES et al., "Cross-Machine Comparison of Resonant Field Amplification and Resistive Wall Mode Stabilization by Plasma Rotation," *Phys. Plasmas*, **13**, 056107 (2006).

94. T. C. HENDER et al., "Prediction of Rotational Stabilisation of Resistive Wall Modes in ITER," *Proc. 21st Int. Conf. Fusion Energy*, Chengdu, China, EX/P8-18, IAEA, Vienna, Austria (2006) (CD-ROM).

95. H. REIMERDES et al., "Reduced Critical Rotation for Resistive-Wall Mode Stabilization in a Near-Axisymmetric Configuration," *Phys. Rev. Lett.*, **98**, 055001 (2007).